**Naval Research Laboratory**

Washington, DC 20375-5320

# Geotechnical and Geoacoustic Investigation of Seafloor Sediments on Boston Harbor Approaches

Andrei Abelev

*Marine Physics Branch*
*Marine Geosciences Division*

Peter Herdic

*Physical Acoustics Branch*
*Acoustics Division*

Michael Vermillion

*Marine Physics Branch*
*Marine Geosciences Division*

Daniel Amon

*Physical Acoustics Branch*
*Acoustics Division*

January 25, 2017

# REPORT DOCUMENTATION PAGE

| 1. REPORT DATE *(DD-MM-YYYY)* | 2. REPORT TYPE | 3. DATES COVERED *(From - To)* |
|---|---|---|
| 25-01-2017 | Memorandum Report | |

**4. TITLE AND SUBTITLE**

Geotechnical and Geoacoustic Investigation of Seafloor Sediments on Boston Harbor Approaches

**5a. CONTRACT NUMBER**

**5b. GRANT NUMBER**

**5c. PROGRAM ELEMENT NUMBER**
74-6907-A7

**6. AUTHOR(S)**

Andrei Abelev, Peter Herdic, Michael Vermillion, and Daniel Amon

**5d. PROJECT NUMBER**

**5e. TASK NUMBER**

**5f. WORK UNIT NUMBER**

**7. PERFORMING ORGANIZATION NAME(S) AND ADDRESS(ES)**

Naval Research Laboratory
4555 Overlook Avenue SW
Washington, DC 20375-5320

**8. PERFORMING ORGANIZATION REPORT NUMBER**

NRL/MR/7420--17-9707

**9. SPONSORING / MONITORING AGENCY NAME(S) AND ADDRESS(ES)**

Office of Naval Research
One Liberty Center
875 North Randolph Street, Suite 1425
Arlington, VA 22203-1995

**10. SPONSOR / MONITOR'S ACRONYM(S)**

ONR

**11. SPONSOR / MONITOR'S REPORT NUMBER(S)**

**12. DISTRIBUTION / AVAILABILITY STATEMENT**

Approved for public release; distribution is unlimited.

**13. SUPPLEMENTARY NOTES**

**14. ABSTRACT**

The report discusses results of free-fall penetrometer and field sampling and analysis series for classification and characterization of the surficial seafloor sediment in the Boston Harbor approaches.

**15. SUBJECT TERMS**

| | |
|---|---|
| STING | Geotechnical |
| Grab sampling | Acoustic character |
| Grain-size analysis | |

| 16. SECURITY CLASSIFICATION OF: | | | 17. LIMITATION OF ABSTRACT | 18. NUMBER OF PAGES | 19a. NAME OF RESPONSIBLE PERSON |
|---|---|---|---|---|---|
| **a. REPORT** Unclassified Unlimited | **b. ABSTRACT** Unclassified Unlimited | **c. THIS PAGE** Unclassified Unlimited | Unclassified Unlimited | 46 | Andrei Abelev |
| | | | | | **19b. TELEPHONE NUMBER** *(include area code)* (202) 404-1107 |

Standard Form 298 (Rev. 8-98)
Prescribed by ANSI Std. Z39.18

## Table of Contents

## Introduction and study location

This report discusses

The coordinates of Box 1 were as follows:

| Field | Latitude | Longitude |
|---|---|---|
| NW Corner | -70.86666667 | 42.44166667 |
| NE Corner | -70.85416667 | 42.44166667 |
| SE Corner | -70.85416667 | 42.4325 |
| SW Corner | -70.86666667 | 42.4325 |

NAVOCEANO databases classify the entire area of Box 1 as silty sand (SM) – as shown in Fig. 3.
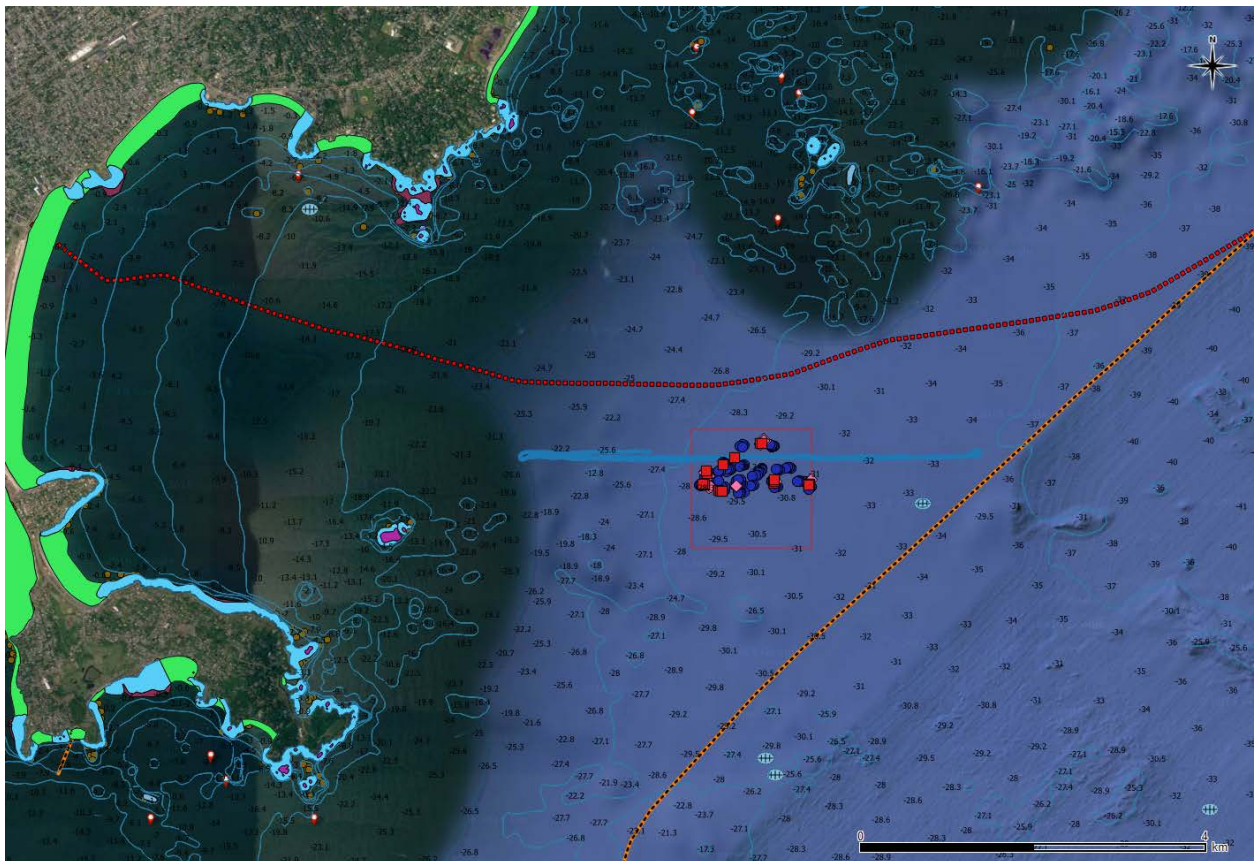


**Fig. 1 General location of the Box 1 study area, including Google<sup>TM</sup> imagery overlay as well as elements of the DNC (Digital Nautical Chart). Also included are preliminary position and actual test locations during BOS16 field collects.**
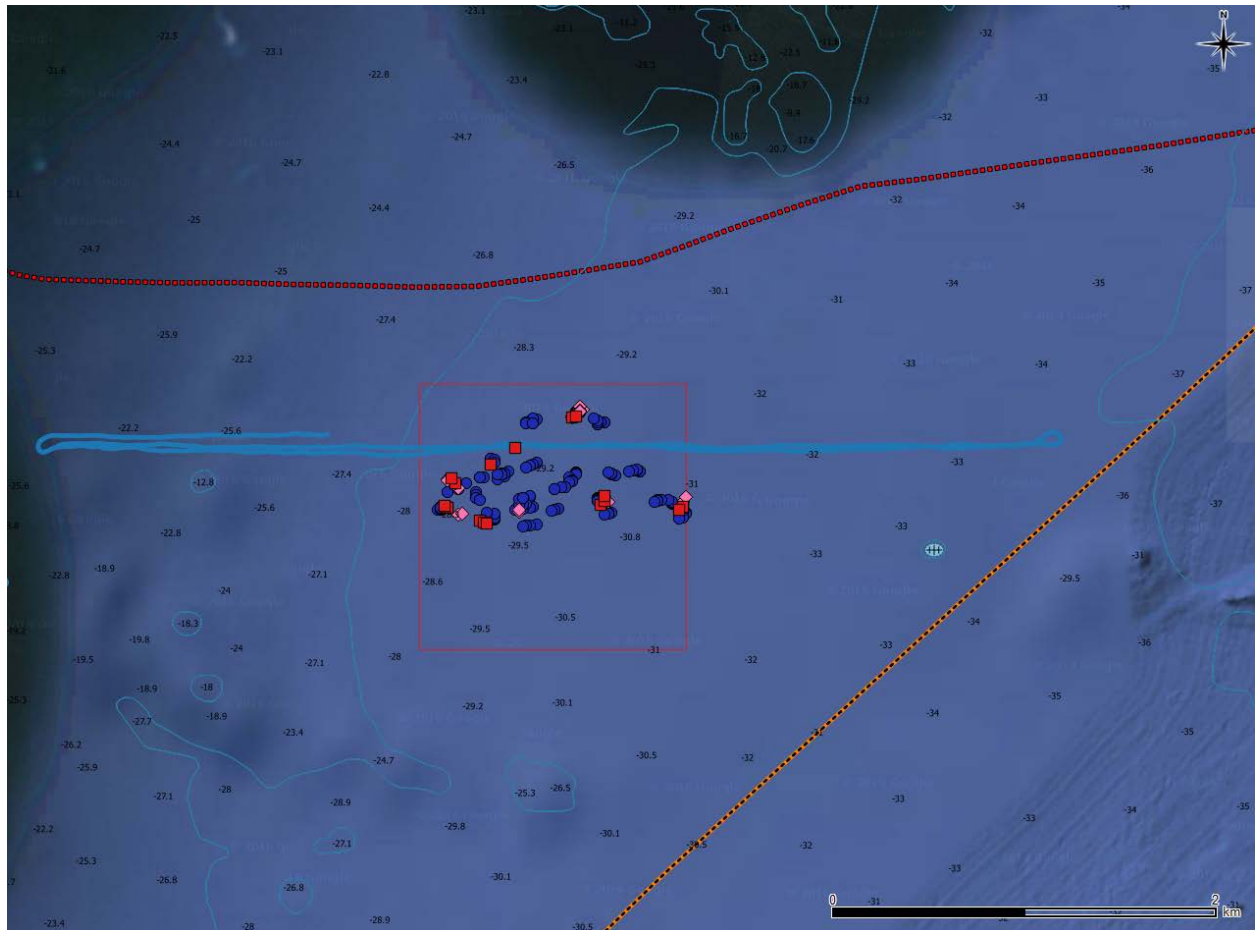
**Fig. 2** Close-up of the test location (Box 1), including Google[TM] imagery overlay as well as elements of the DNC, including DNC-included seafloor sediment description. Planned position deployment grid and actual test locations during BOS16 field collects are also shown. The series of long horizontal lines are vessel track during the anchor chain drag through the test box.
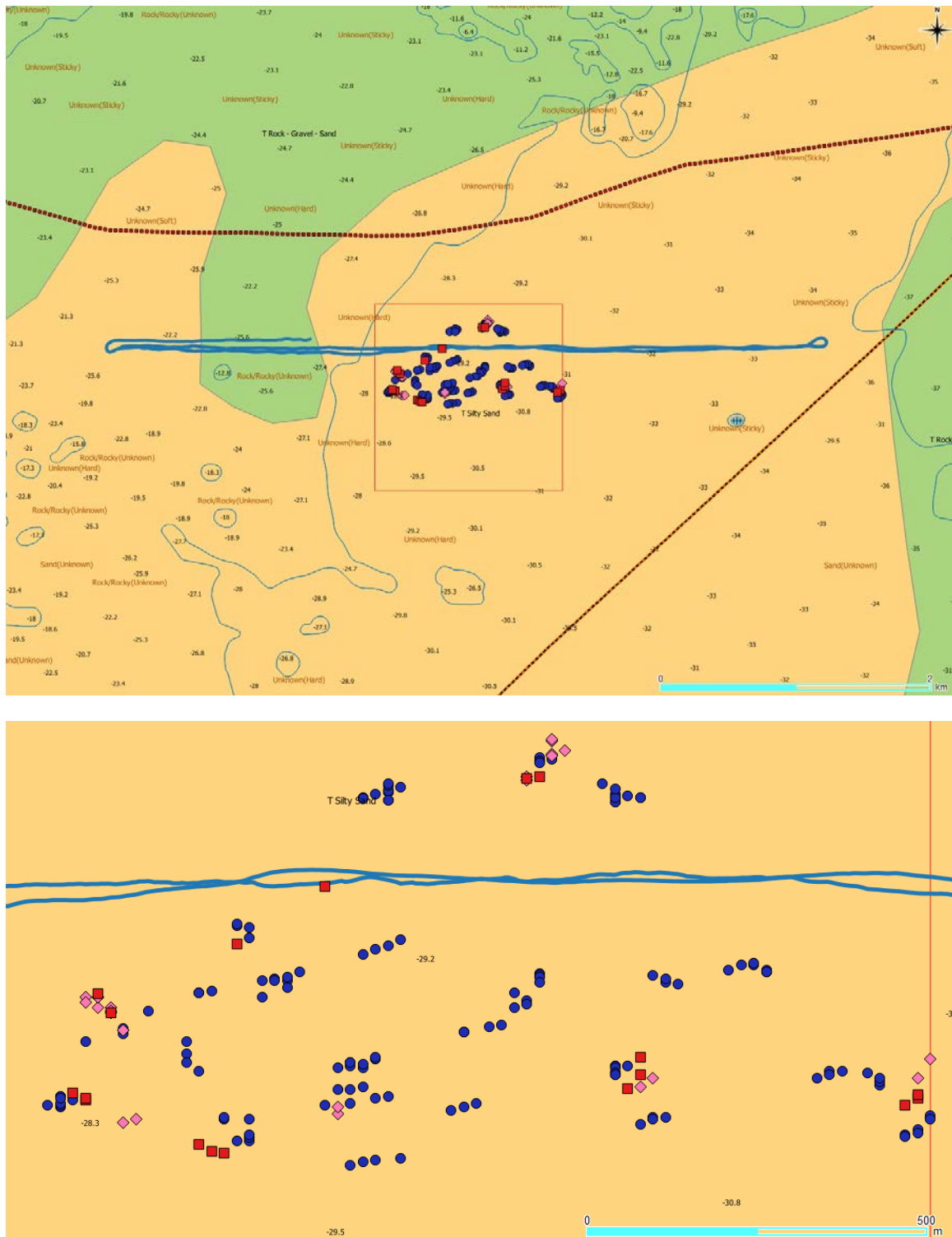
2

**Fig. 3** Overall view of the test location (Box 1) and a close-up, including elements of the DNC. Blue Dots are STING drops, Red Squares are Sediment Grabs, and Pink Diamonds are Object drops (mine-like and generic shapes). Long horizontal lines represent vessel track during the anchor chain drag.

**Instrumentation**

A set of three 7420 STINGs (Sea Terminal Impact Naval Gradiometer - Jasco Research Ltd. 2002) was used in conducting sediment analysis for bearing strength.  These probes consist of a fin-stabilized main body with extension/penetrator rods attached to it.  Several diameter foot-plates can be attached to the bottom (penetrating) end of these extension rods, including 25, 35, 50, and 70mm diameter.  The main body of the probe includes a single axis accelerometer, water pressure transducer, and data acquisition and storage unit with the total on-board memory sufficient for 4.5 min data acquisition, when recording in dual-channel mode (acceleration and water pressure).  During this time interval, repeated drops of the penetrometer are conducted at each station to provide for averaging necessary in naturally heterogeneous seafloor sediment conditions.  Normally, three to four drops per location were performed.

Selection of the STING foot diameter may be guided by several considerations, including intended depth of penetration where the smaller the foot diameter, the greater is the resulting penetration burial thus maximizing the depth surveyed with the probe; the quality of data used in correlations with the sediment undrained shear strength as some diameters may yield better modeling outcomes due to a variety of soil plastic flow effects around the penetrometer foot; or direct empirical relations between the maximum depth of the penetrating probe with expected depth of burial of larger objects.  These size effects were studied with several penetrometers of varying dimensions (Mulhearn 2002) and showed that little change in maximum burial occurs for circular bodies of diameter greater than 70 mm.  During this survey, a 75mm foot was utilized, to utilize these direct correlations.

In general, the numerical model used in retrieving the sediment strength from deceleration records of probes is applicable to cohesive materials (clays and silts) or mixtures that exhibit a mostly cohesive behavior.  If large enough layers of sandy material are present, they result in characteristic spikes in acceleration (and this bearing strength) records, due to the dilative effects in the sandy material matrix.  These layers need not be clean sand to impose this effect and are most likely a mixture with surrounding finer-grained material (silt and clay).  These dilative effects, however, may severely impede penetration of various objects, especially when the impact velocities are high (*e.g.* greater than 1 meter per second) relative to the overall sediment permeability or the ability to dissipate excess pore water pressures quickly.  For further information on the effects of dilation on dynamic penetration, the reader is referred to Stoll et al. 2007.

The range of the accelerometer, used in the STINGs is chosen in such a way as to maximize resolution in investigating mostly cohesive/clayey soils.  When significantly higher resistance is encountered in sandy layers, the accelerometer often saturates, exceeding the range.  Part of the calculation may still be conducted, retrieving the pseudo-strength values, but these should be treated with care, as they lay outside the normal range of the sediment strength retrieval model.

## Results: Sediment sampling and grain-size analysis

Sediment sampling was undertaken during the field trials by utilizing a small grab sampler, with manual deployment.  Due to the relatively stiff surface sediment composition (silty sand with some gravel) as well as strong winds and currents during the sampling, only a limited number of effective grabs has been accomplished.  In one instance (position markers 39 and 41), ship's drift was severe enough to move the aggregate sampling point approximately 110m.  Stiff sediment resulted in only small amounts of material retrieved each time, thus the necessity of repeated Grab sampler deployments to accumulate volumes sufficient for subsequent laboratory analysis.  Other locations also required multiple grab deployment but were less hampered by excessive vessel drift, thus producing sediment sampling windows of maximum of 38m in diameter.  Sample 8 (position ID 135) was of minimal size needed for lab processing, with the processing outcome potentially biased as a result.

A total of 7 samples were retrieved and analyzed in the lab.  This analysis included mechanical sieving – a standard grain-size characterization technique (ASTM Standard D422-63 2007).  Sediment classification was performed according to the standard geotechnical procedure (ASTM Standard D2487 2010) – a Unified Soil Classification System.  The overall results of the tests are shown in Table 1, including average locations (averaged over several sampling spots
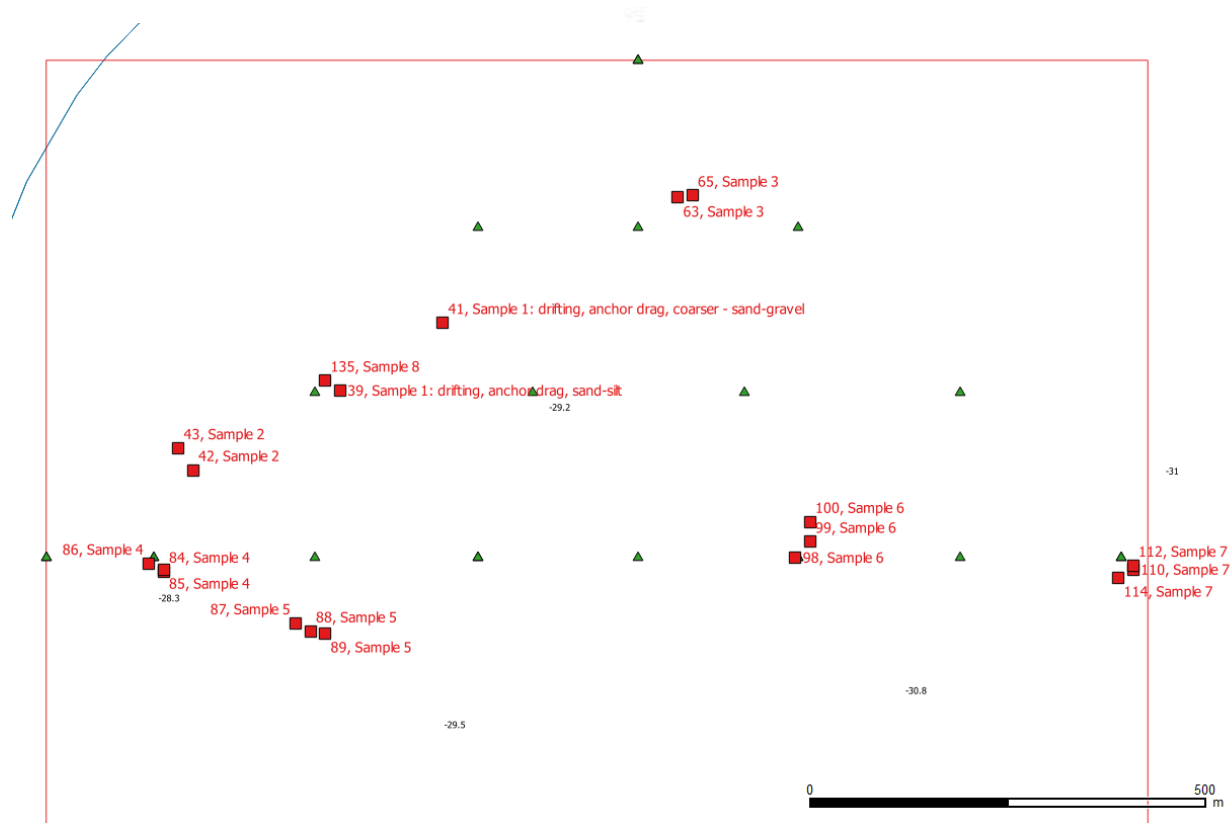


**Fig. 4  Grab sampling locations (Red Squares) are shown together with GPS position IDs and nominal grid locations (Green Triangles).  Several grabs represent a single sample, analyzed in the lab.**

5

that contributed to the same sample).

**Table 1  Results of sediment classification from laboratory grain-size analysis**

| Sample ID | % Gravel | % Sand | % Fines | $D_{50}$, mm | USCS class | USCS full | Lat_deg | Lon_deg |
|---|---|---|---|---|---|---|---|---|
| Sample1 | 20.37 | 78.32 | 1.31 | 0.68 | (SP-SM)g | Poorly-graded Sand with Silt and Gravel | 42.43918 | -70.8628 |
| Sample2 | 11.17 | 80.15 | 8.68 | 0.22 | SP-SM | Poorly-graded Sand with Silt | 42.43833 | -70.8651 |
| Sample3 | 19.27 | 80.46 | 0.27 | 2.10 | SPg | Poorly-graded Sand with Gravel | 42.44053 | -70.8594 |
| Sample4 | 11.29 | 84.49 | 4.23 | 0.23 | SP | Poorly-graded sand | 42.43741 | -70.8654 |
| Sample5 | 5.57 | 86.00 | 8.43 | 0.19 | SP-SM | Poorly-graded Sand with Silt | 42.4369 | -70.8637 |
| Sample6 | 10.21 | 84.82 | 4.97 | 0.25 | SP | Poorly-graded Sand | 42.43764 | -70.8581 |
| Sample7 | 2.32 | 84.80 | 12.89 | 0.16 | SM | Silty Sand | 42.43739 | -70.8544 |
| Sample8 | 35.95 | 62.54 | 1.51 | 0.32 | SPg | Poorly-graded Sand with Gravel | 42.43898 | -70.8635 |

## Geotechnical similarity of Box 1

The entirety of the Box 1 explored with the Grab Sampler and analyzed in the lab is similar with respect to the grain-size distribution of the material.  All of the sediments are coarse-grained and all dominated by the sand fraction (75um —4.75mm).  All are poorly-graded, i.e. relatively uniform in grain-size distribution.  Among these samples, however, there is a notable change from East to West along the bottom portion of the explored area (Samples 4 – 7) – with some tendency of slightly higher silt content in the East, transitioning to a more pure sand towards the West.  Sample 3 – the Northern-most location in the box sampled, still qualifies as SP (Poorly-graded Sand) but with a much more noticeable Gravel content, as well as a noticeable difference in the entire grain-size distribution curve (see Fig. 7) and coarser grains in all sub-fractions.  This is also notable in the Mean Grain Size ($D_{50}$, mm), as shown in the table.  Samples 1 and 8 – may be considered a transition zone with progressively higher inclusion of the coarser material, including coarser sand and gravel.  Sample 7 (Eastern-most) has the highest Fines content (almost 13%) as well as the finer distribution within the sand fraction.  The fines are estimated to be mostly Silt.  Fig. 8 shows a plot of sampling locations with the grain-size classification labels.  Exact measurement was not possible due to the sampling method employed and the sea conditions during Grab-sampling, during which, careful retaining of fines within a small sample was not possible.  This assessment would match that from the existing NAVOCEANO databases (Silty-Sand), marked for the entirety of this domain (also see Fig. 3).

Examples of two grain-size analyses are shown in Fig. 5 (Sample 4) and Fig. 6 (Sample 3). There is a noticeable change with increase in the coarser components.
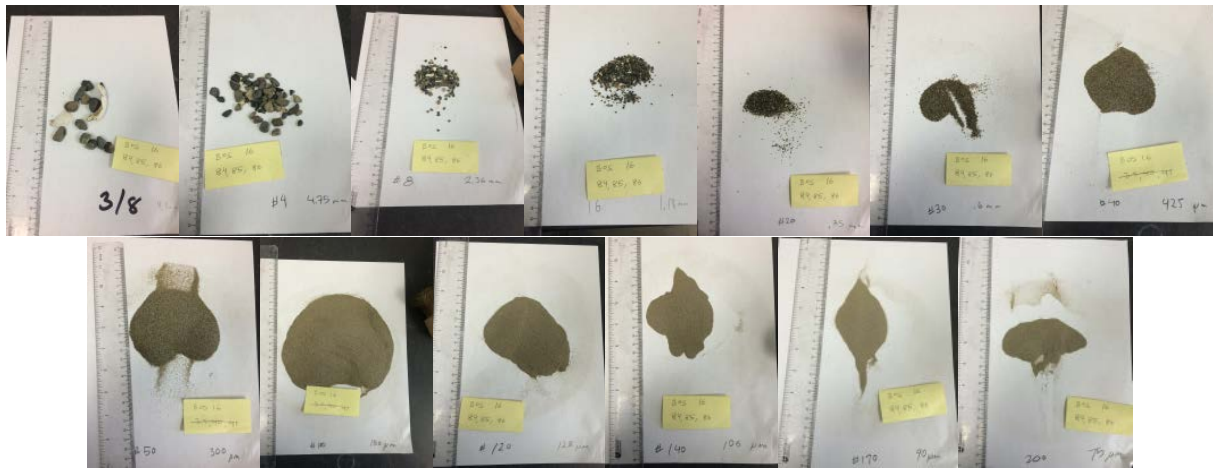


**Fig. 5 Sample 4 (positions 84, 85, 86) "SP" – grain-size by sieve (retaining): 9.5, 4.75, 2.36, 1.18, 0.85, 0.6, 0.425, 0.3, 0.15, 0.125, 0.106, 0.09, 0.075 mm.**



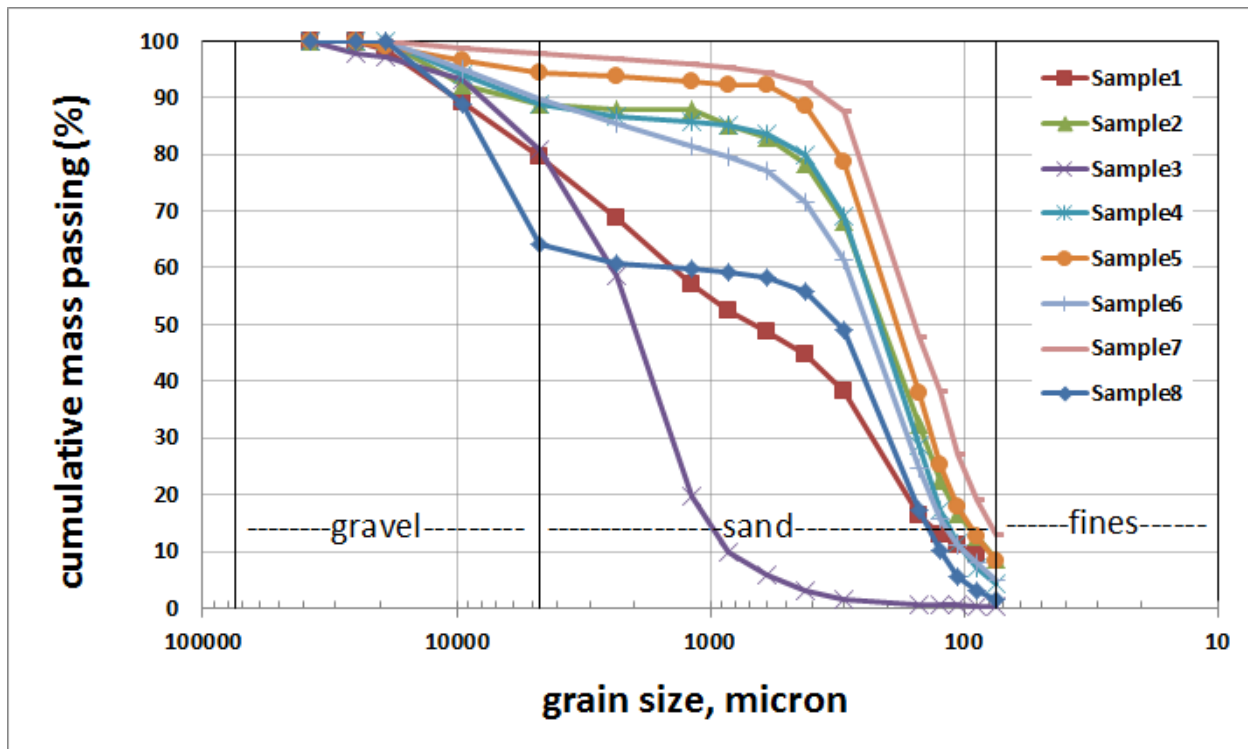**Fig. 6  Sample 3 (positions 63, 65) "SPg" – grain-size by sieve (retaining): 25.4, 19, 9.5, 4.75, 2.36, 1.18, 0.85, 0.6, 0.425, 0.3, 0.15, 0.125, 0.106, 0.09, 0.075 mm.**

**Fig. 7  Grain-size distribution analysis of Grab samples.  Size limits for Gravel, Sand, and Fines (silt and clay) are also shown**
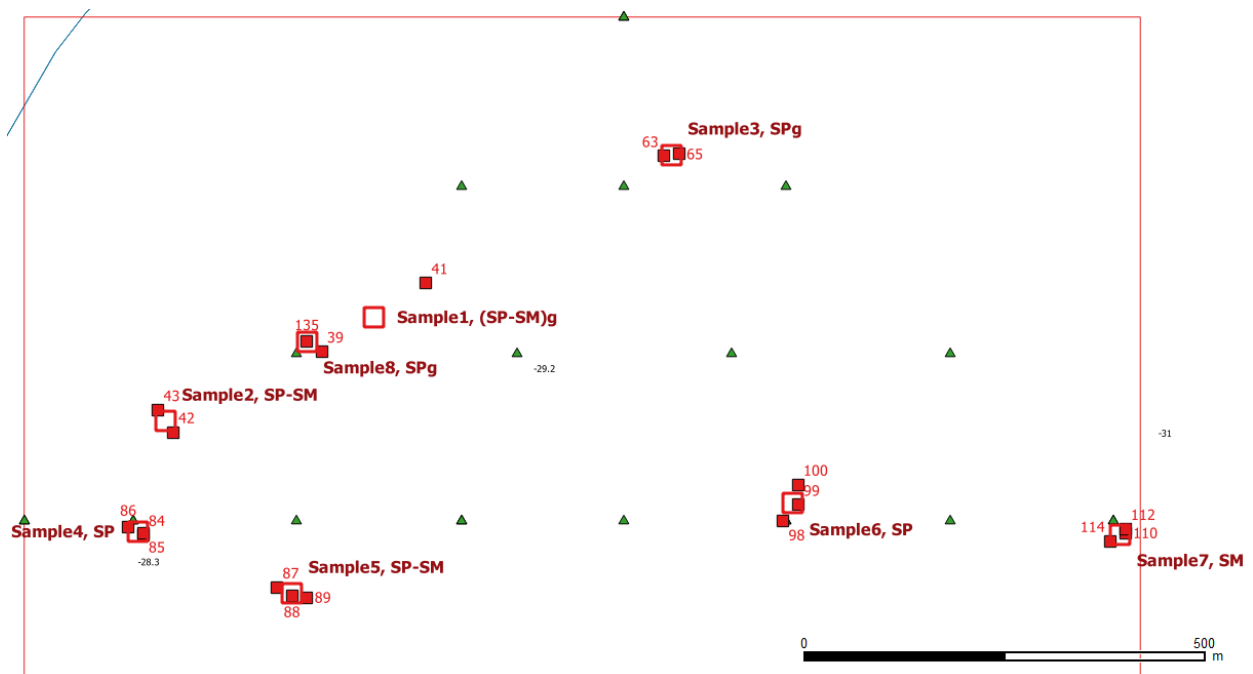


**Fig. 8  Sediment classification according to USCS is shown with an averaged position of all individual Grabs. Slight change from Silty-Sand on the Eastern side of the area to more pure Sand in the West, as well as larger Gravel component toward the Northern-most location can be noted ("S"-Sand, "M" – Silt, "G" – gravel).**

8

## Results: STING penetration and shear strength

The results of the STING deployments are summarized in Table 2.  Each station includes an average of typically three to four STING drops.  Maximum penetration values are shown in the table as well as in Fig. 9,  and include the average of all the drops performed at each station.

It is noticeable, if generating a contour plot of the maximum penetration burial of the 25mm STING (Fig. 10), that the Center-North portion of the examined area is stiffer than the outlying areas, even including the generally coarser Northern-most point.  There was no grab sample taken anywhere near that location, and so no definitive proof of larger particle size sediment near the middle of the domain exists.  Such assumption is reasonable based on the STING drop analysis and relative comparison of the surficial sediment stiffness.

Overall, the combination of the STING probing and the Grab sample-based sediment classification would indicate some degree of surficial sediment heterogeneity, with stiffer and likely coarser-grained material near the center of the domain and toward the North and finer toward the East. STING results indicate that this change may not be gradual throughout the box but include some relatively abrupt changes, as is evident from the results shown in Fig. 10.
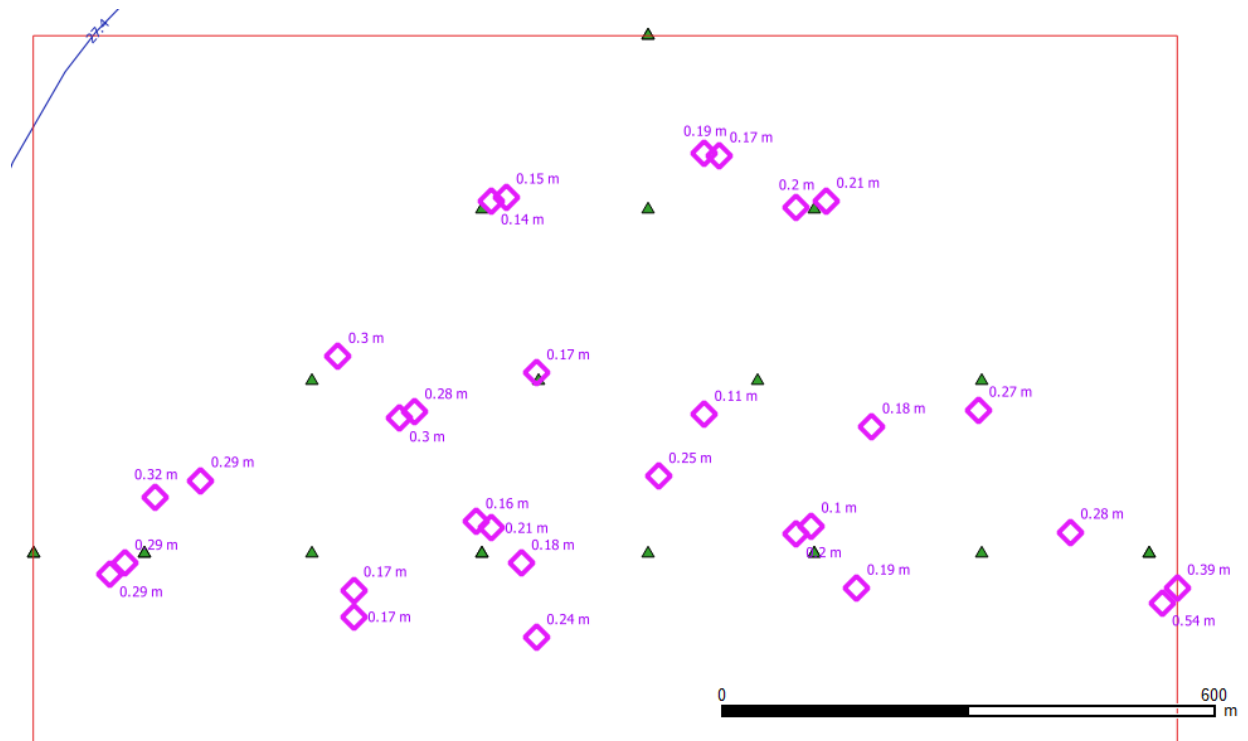


**Fig. 9  Average locations for each STING drop series, with values indicating average Maximum penetration of a 25mm foot (in meters). Green triangles indicate nominal target stations for STING survey**
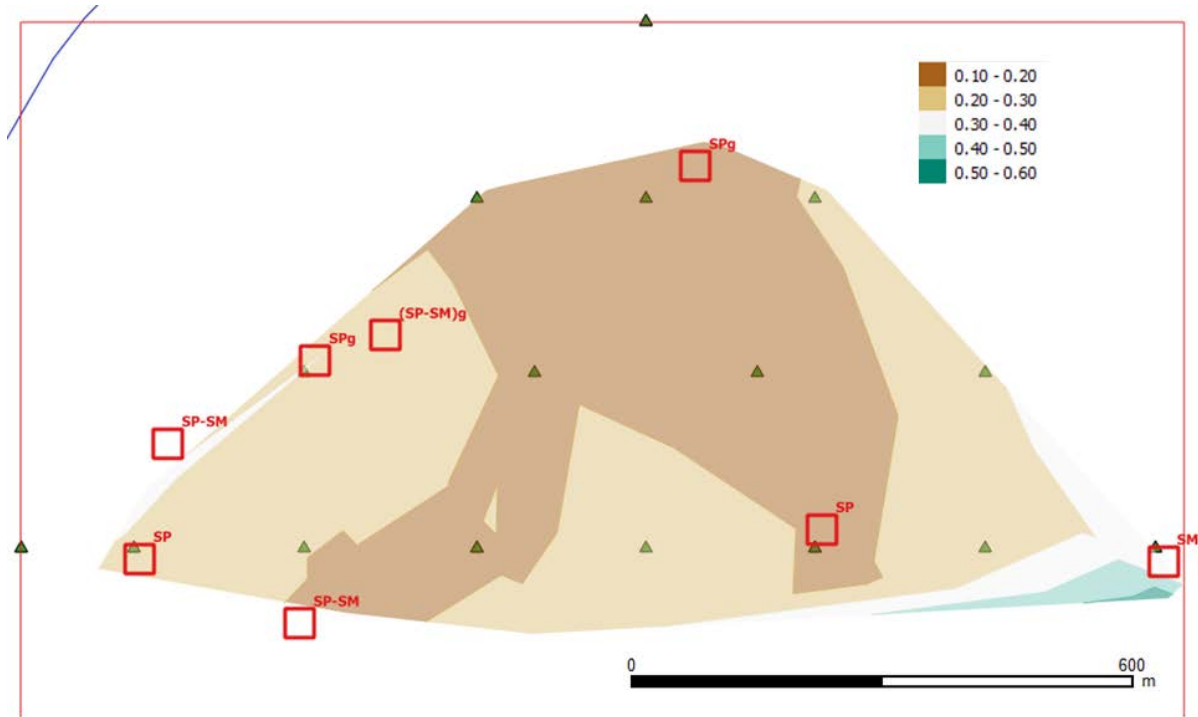
**Fig. 10 Approximate contour of maximum (average) STING 25mm penetrations – Blue: greater, Brown: smaller. Red Squares represent the average Grab Sample locations and sediment class (USCS) determined. Sample nomenclature (standard USCS – Unified Soil Classification System, ASTM): SP – Poorly-graded Sand, SPg – Poorly-graded Sand with gravel, SP-SM – Poorly-graded Sand – Silty Sand mixture, SM – Silty Sand, (SP-SM)g, Poorly-graded Sand and Silty Sand with some gravel.**

## Extending sparse Grab Sampling data using STING data set

One could use a larger and denser point-cloud generated by the STING surveys as a proxy of sediment response, and then, extrapolate the $D_{50}$ from only eight points to the entire survey area. An interpolation could be done by first conducting a gridding operation on the sparse grab sample data and then retrieving the values of the gridded variable (from STING data) that correspond to the Grab Sample variable of interest ($D_{50}$). The choice of the STING-derived variable may vary, e.g., a maximum depth of penetration. If we attempt such a correlation, we will notice that there is no unique relation between maximum depth of STING burial and the average grain size of the sediment. These results are shown in Fig. 11.

There are several reasons for the apparent lack of correlation. First, the complexity of the sediment grain-size composition is poorly described by the mean grain size only. At the minimum, additional parameters are needed, e.g. coefficient of uniformity ($C_U$) and the Coefficient of Curvature ($C_C$) or, alternatively, additional curve parameters, such as Percent Gravel, Percent Sand, Percent Fines (Silt and Clay). There are no known correlations in literature that attempt to relate acoustic properties of the sediment to such more complex grain-size curve descriptions. We are thus forced in using mean grain size only.

Additionally, the value of the STING maximum burial may not be a good representation of the sediment sampled using the grab sampler – i.e., the sediment exhibits variability with depth that is not captured by the shallow sampling. This sampling in our case, was particularly shallow due to the small size of the grab sampler, the stiff nature of the sediments, and the difficult sea conditions resulting in large drift of the vessel during sampling, resulting in many empty grabs retrieved.

Alternatively, instead of the maximum STING penetration values, we can explore the sediment represented by perhaps only top 5cm, the expected maximum Grab sampling depth. If so, we could devise a variable representing such surficial layer of the sediment, based on the STING records. Here, we attempt to use the following variable:

$$BS_{ave5cm} = L^{-1} \int_{0cm}^{5cm} BS(z)dz , \qquad (1)$$

where $BS$ is the Bearing Strength, as calculated by the STING algorithm, $L$ is taken as 5cm or the integration depth, and $z$ is the depth in the sediment. The variable represents an average Bearing Strength over this depth profile and is a measure of energy dissipation of the free-falling STING probe. This energy dissipation is related to sediment strength (dynamic strength)
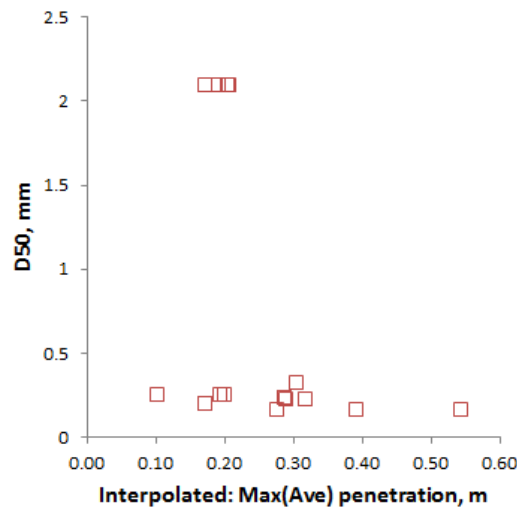


**Fig. 11  Mean grain size of the grab samples ( $D_{50}$ ) vs. the interpolated points based on maximum penetration distribution of the 25mm STING in Box 1**
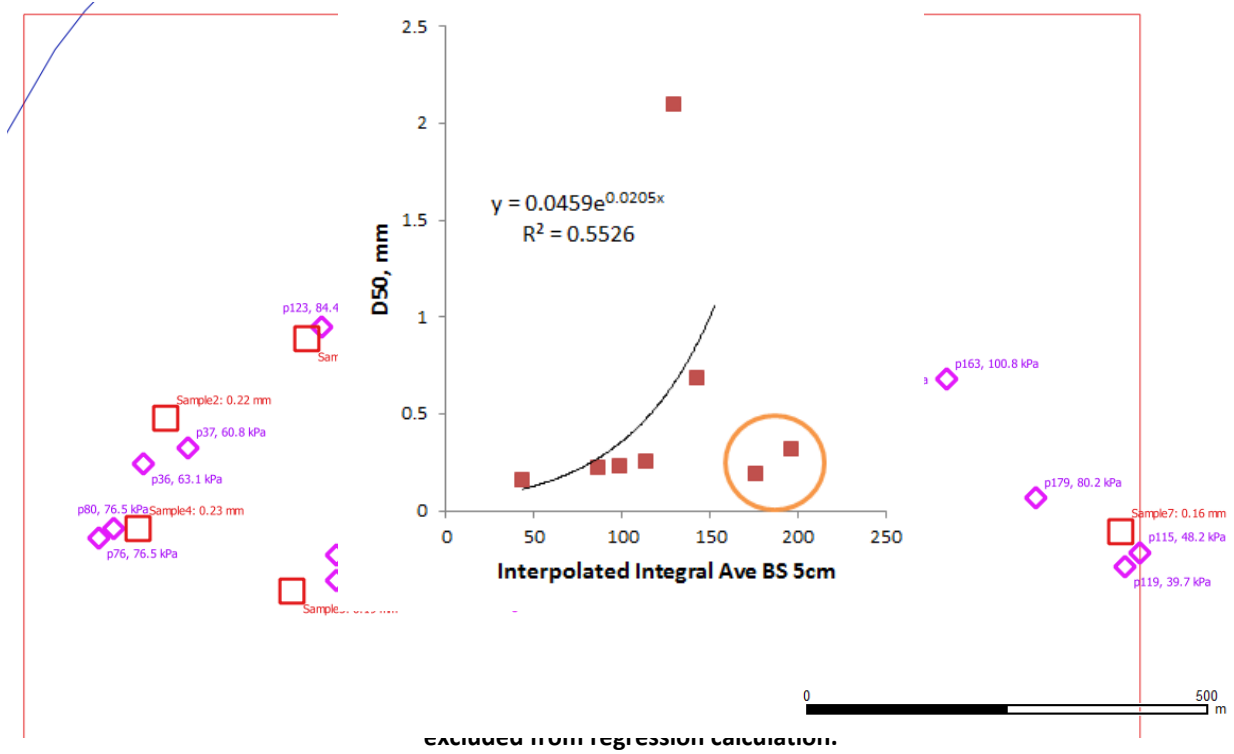
11

**Fig. 12. STING locations with position IDs and values of the average Bearing Strength values over top 5cm of sediment (magenta diamonds, units: kPa) as well as the grab sampling averaged locations together with the lab-determined mean grain size (D50, in mm).**

and is indirectly related to the consistency of the sediment, one of which may be expressed via its drain-size distribution.

 shows the two data sets: STING mean bearing strength over top 5cm, together with the positions of the sting drop sequence as well as the Grab Sampling set together with the values of the mean grain size parameter ($D_{50}$). In general, for surficial marine sediments, we can expect higher values of the dynamic bearing strength, as determined by a free-fall probe such as STING, in coarser sediments, i.e. sediments with higher values of the mean grain-size , $D_{50}$. shows the results of interpolation for Box 1 based on the Grab Sampler Mean Grainsize values. Then,  suggests a possible, albeit weak, relationship between the mean bearing strength of a surface layer and the mean grain size.  The correlation is still not a strong one, but would be supported by a generally expected relationship, where the greater is the average material grainsize is, the higher the seafloor sediment strength (as measured by the free-falling probe, such as STING) may be expected to be.  It is possible that due to the small size of the grab sampler, the surficial material characterized in the lab may in some instances be mis-characterized due to un-representative sampling.

Thus, if such a relationship were to exist, it could be expressed by an exponential curve, e.g. as indicated in the figure:

$$D_{50} = 0.046e^{\left(0.0205\,BS_{ave5cm}\right)}. \tag{2}$$

12

In this case, however, the accuracy of correlations is insufficient to suggest the general applicability of such a relation.

The results shown demonstrate that while the accuracy of the correlations is low, there is an observable tendency toward coarser material in the Northern and apparently North-Central parts of the Box 1.  This relates not only to the mean grain size but also to the entire material size distribution as noted earlier in the analysis of the grab lab analyses, resulting in higher gravel concentration and coarser sand fraction (primary component).  We can further attempt to use the combined set of values of the mean grain-size ($D_{50}$) from Grab Sample analysis as well as those computed using Eg. (4) based on the STING results, as a basis of interpolation for the entire domain.  Results of such an interpolation are given in .

Additionally, a data set is available from USGS (Pendleton et al. 2005) derived from a seismic survey.  The data published is of a somewhat coarser resolution within the test box, but it does, however, confirm the general sediment composition and presence of finer material in the S-E corner of the domain explored – identifying it as "very fine sand".  These data is shown in .

In general, the extrapolation of the mean grain-size data using STING results is generally noisy and of relatively low confidence for high-accuracy estimates.  The material within the survey box appears highly heterogeneous.  The results do suggest however, especially, when combined with the historical analysis (Fig. 15) that the sediment is generally coarser in the North and perhaps North-Central areas of the box.  Here the sand includes a progressively more substantial gravel component, especially the Northern most point explored.  It is relatively uniform (without obvious large variations) throughout the remainder of the box surveyed, with the notable exception of the extreme East corner where the sediment changes to a finer Sand-Silt mixture, from the otherwise Sand with some gravel presence.
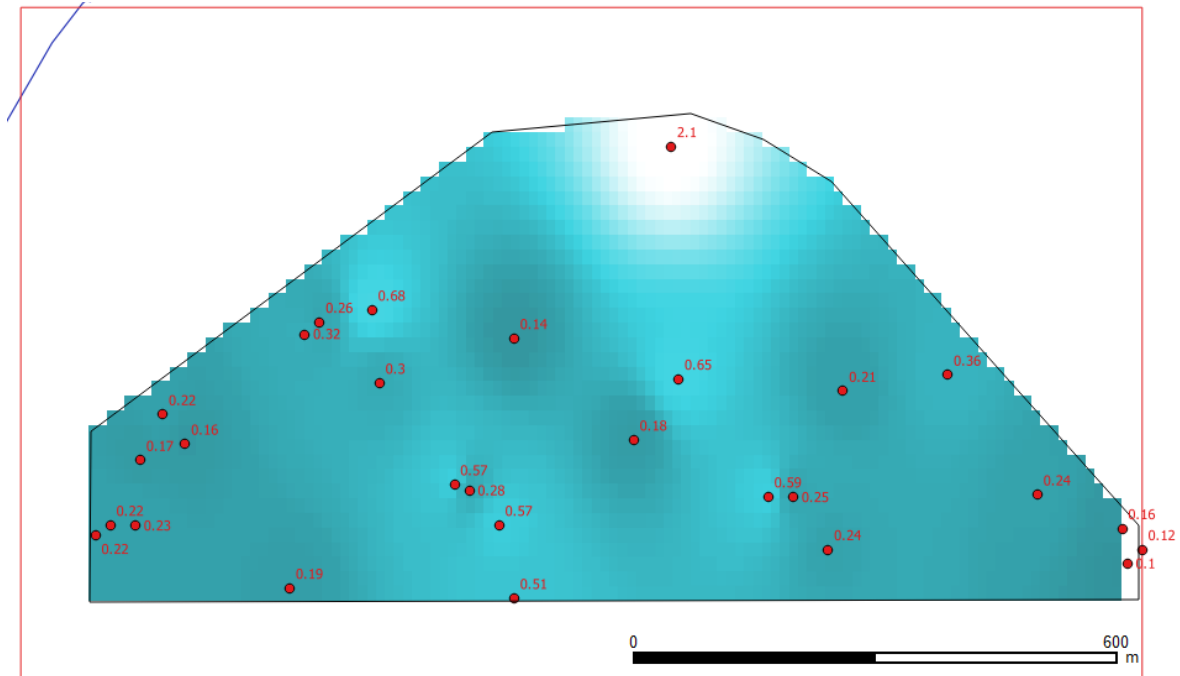
**Fig. 14  Approximate intensity map of Mean Grain-size (D$_{50}$, mm), extrapolated based on the values of the Grab Samples and computed values of D$_{50}$ from STING burial according to Eq. (4)**
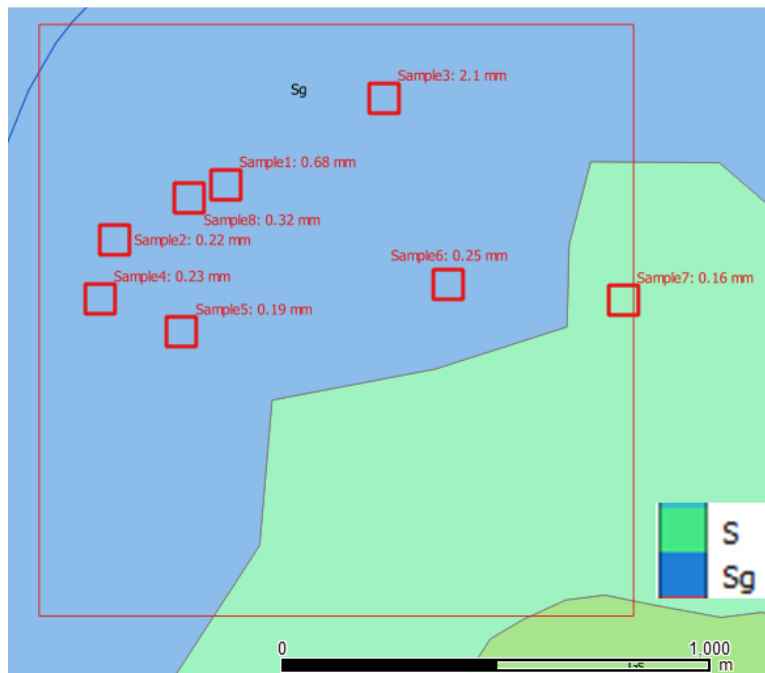


**Fig. 15  Sediment domains, showing Sg (Sand with gravel) – Blue, and S (Sand – Very fine sand) – Green.  Inferred from the seismic profiling (Pendleton et al. 2005)**

14

## Geotechical – acoustic correlations

In general, correlations between sediment classification and acoustic propagation properties can be made. These correlations, however, should not be expected to be very precise, if no locally measured sound speed velocity and attenuation measurements have been made on retrieved undisturbed sediment samples (see, e.g., an experimental setup in Fig. 16). If such data were available in at least some locations within the domain, these could be extrapolated based on other available sediment profiling data, e.g. STING probing, Grab sampling and grain-size analysis. Lacking these more accurate measurements, only a range of values can be estimated for each soil type and for each frequency range of interest. In this report, we will consider two frequency ranges: "slow" – 10-30 Hz, and "fast" – 0.5 – 5.5 kHz.

*Approach 1*
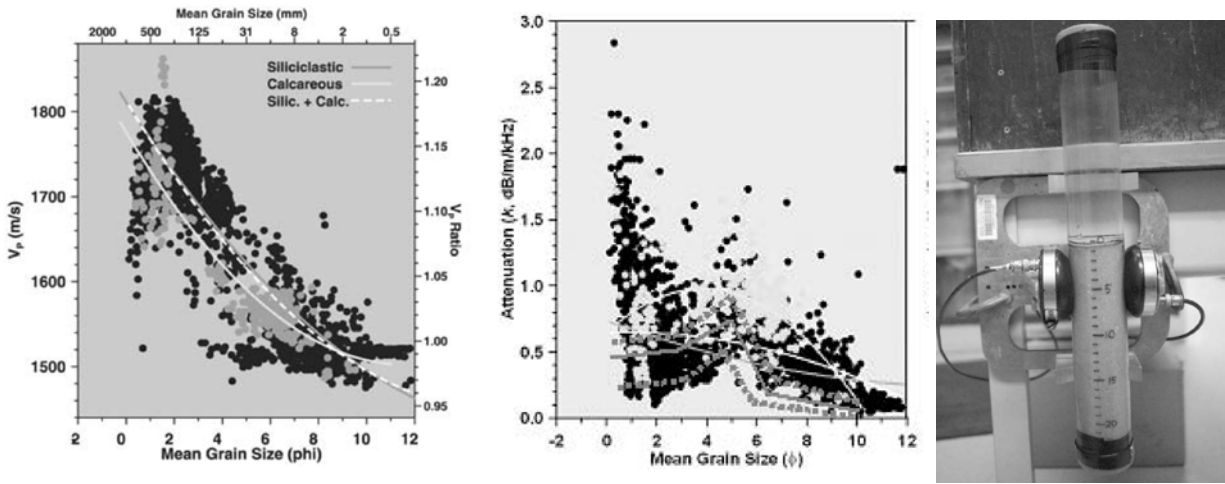


**Fig. 16 Sound speed (and Sound speed ratio) and Attenuation coefficient in sediments of various origin as function of the mean grain size (Jackson and Richardson 2007 p. 136), expressed in** $\phi = -\log_2(D_{50}[mm])$. **The experimental setup is shown on the right.**

An empirical equation of the sound speed ratio ($V_p R$), or the ratio of the sound speed in sediment to the sound speed in water was compiled (Jackson and Richardson 2007) for several sediment classes, of which, siliciclastic sediment class is applicable:

$$V_p R = 1.184 - 0.028 D_{50} + 0.0008 D_{50}^2 .$$ (3)

where $D_{50}$ - is the mean grain size, expressed in units of $\phi$:

$$\phi = -\log_2 D ,$$

where $D$ is the grain-size in [mm].

The attenuation factor $k = \alpha_p / f$ [dB·m$^{-1}$·kHz$^{-1}$] is also represented by a general empirical equation:

$$k = 0.74 - 0.07 D_{50} - 0.02 D_{50}^2 ,$$ (4)

albeit with a very poor overall fit, as is evident from Fig. 16. The figure shows the experimental data and the empirical fits for both quantities. The data was compiled using tests at 400kHz, with direct acoustic transmissions through an undisturbed sediment core (normally retrieved by divers). It is obvious that the equation for the velocity ratio only represents a range of possible values that can vary by 100-150m/s. In our case, the values of the compressional velocity is approximately within the 1600-1900 m/s range for sand-silt mixture on one end to coarser sand and fine gravel on the other, respectively.

In the case of the attenuation factor, the overall fit is rather poor, especially for the coarser materials with the values of $\phi$ between 0.5 and 3 (equivalent to particle diameters of 0.7—0.125mm). There is no available data for values lower than about $\phi = 0.5$. Unfortunately, a substantial portion of the materials sampled in the test area are very close to this value.

Alternative evidence published (Hamilton 1976) suggests a range of attenuation factors *k* for the sediment with the mean grain size as measured here is approximately $0.2 - 0.5$.

## Shear wave speed

Similar to the compressional wave speed, we could estimate the shear wave speed based on the published correlations with the mean grain-size diameter of the sediment (Fig. 17). The range of grain-sizes (approximately from -1 to +3 in our case) represents a range of shear speed
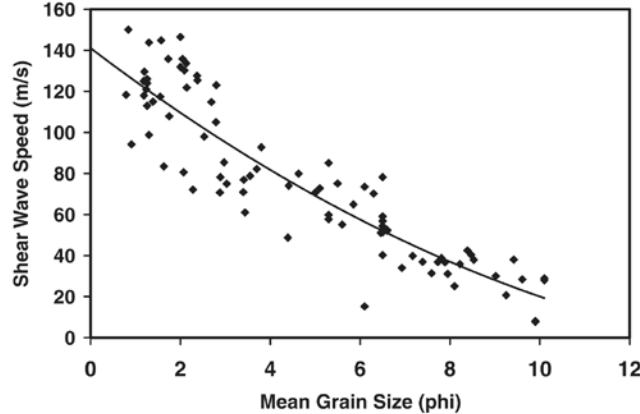


**Fig. 17 Shear wave speed vs. mean grain size from Jackson and Richardson 2007 p. 158. The relation is valid for both carbonate and siliciclastic sediments**

of approximately 80-100m/s in silty-sand material of Box 1 (SE corner) to about 140-160 m/s in the coarser sand-gravel mixture in the Northern and (apparently) North-Central zones.

There is also evidence to suggest that these values vary with depth (Hamilton 1976, Jackson and Richardson 2007). The suggested relation of $V_s$ with depth is of the following type:
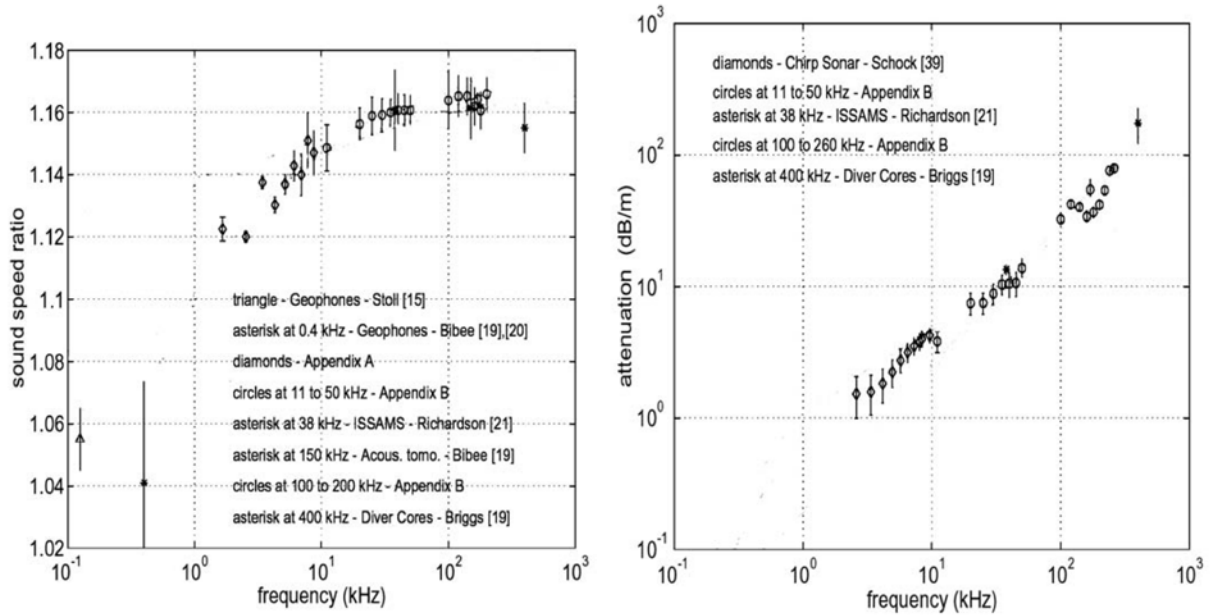
$$V_s = aD^b,$$ (5)

**Fig. 18 Dependency of sound speed and attenuation on frequency according to the data compiled by Williams et al. 2002.**

where $a$ is between [130—190] and the exponent $b$ is [0.27—0.28].  Alternative relations exist, including linear variations with depth, but they tend to produce higher errors for the very surficial shallow layer of the sediment and are thus less appropriate for our correlations.

## Sound speed and attenuation as functions of frequency

Much of the evidence present above is based on work at higher frequencies, especially 400kHz. There is a clear dependency of sound speed and attenuation on frequency, e.g. as given in Fig. 18.  These data would suggest that the sound speed would appear approximately constant down to about 30kHz and then a constant decay of the sound speed ratio by about 0.4—0.5 for every log-cycle of frequency.

Attenuation shows a power law decay, constant over the entire frequency range explored and about an order of magnitude (in dB/m) decay over an order of magnitude reduction in frequency (in kHz).   Additional evidence published (Hamilton 1980) suggest a similar reduction of the attenuation with frequency.

## Density

Density determinations based on the Grab Sampling is not possible, as the material retrieved is disturbed with no possibility of controlling the sampling volume or preserving it during the retrievals.  Thus, we could make some general estimates of the bulk density of material in Box 1

based on the available literature and considering the Grab-determined Sediment class and grain-size distribution.

General ranges of the bulk density for various soil types (Hamilton 1980 and Clay and Medwin 1977 p. 259) suggest that the material in Box 1 varies from approximately 1.800 gr/cm$^3$ for the silty sand (in SE corner) to approximately 2.050 gr/cm$^3$ for the coarsest material present – coarse grained sand with fine gravel in the North and North-Central portions.

## Stratigraphy and sediment depth to bedrock

Acoustic propagation modeling also requires a definition of the proper boundary conditions – including sediment stratification, if known, and distance to bedrock. Field sampling and surveys, performed during the trials, did not address this directly. There are, however, historical data available that can answer some of these questions. One such USGS report contains detained survey data from interferometric and sidescan sonar, and chirp seismic-reflection [Barnhardt et al. 2006].
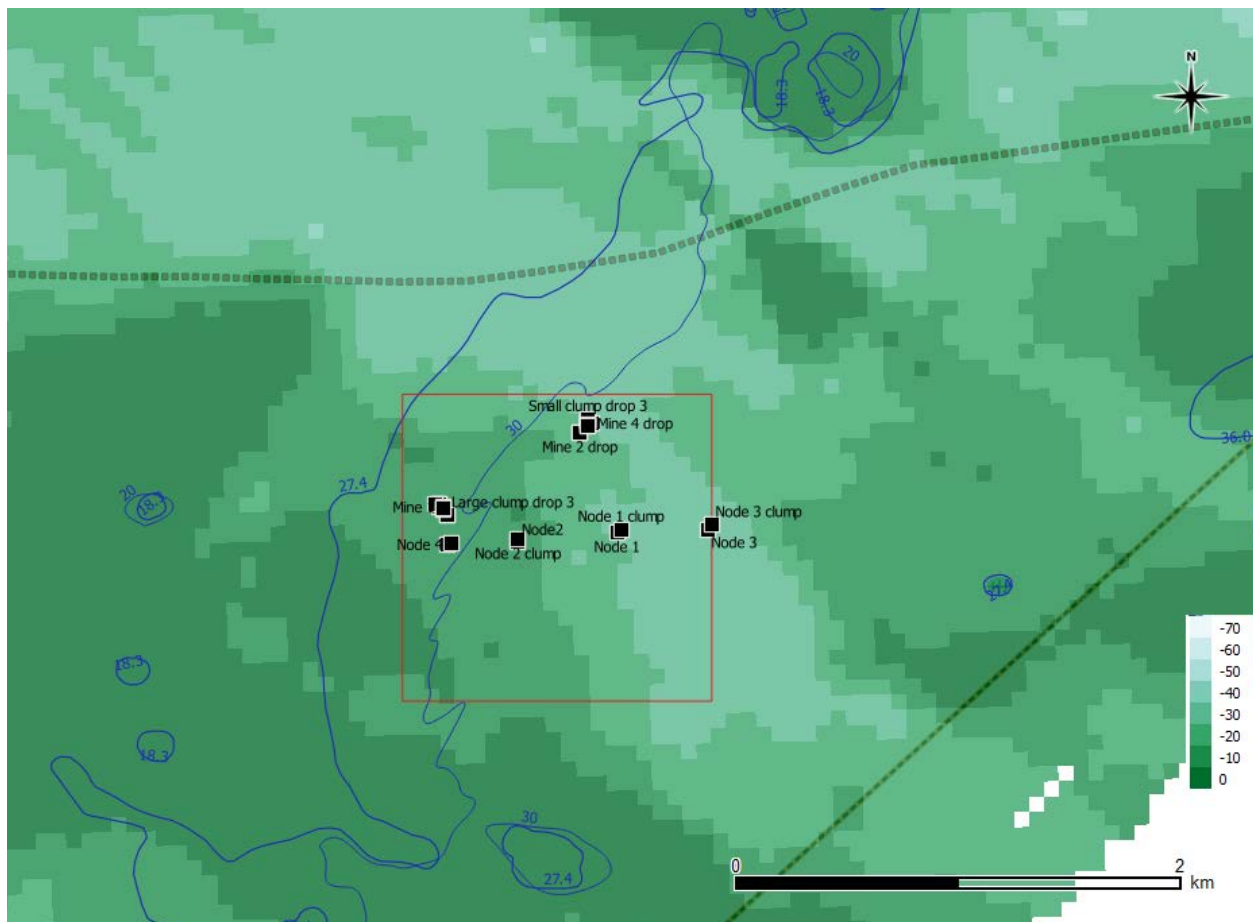


**Fig. 19 Sediment depth to bedrock, as determined from chirp seismic profiling [Barnhardt et al. 2006] (Scale is in meters). Main survey box is outlined as well as the positions of the mine and clump-weight drops and the node positions.**
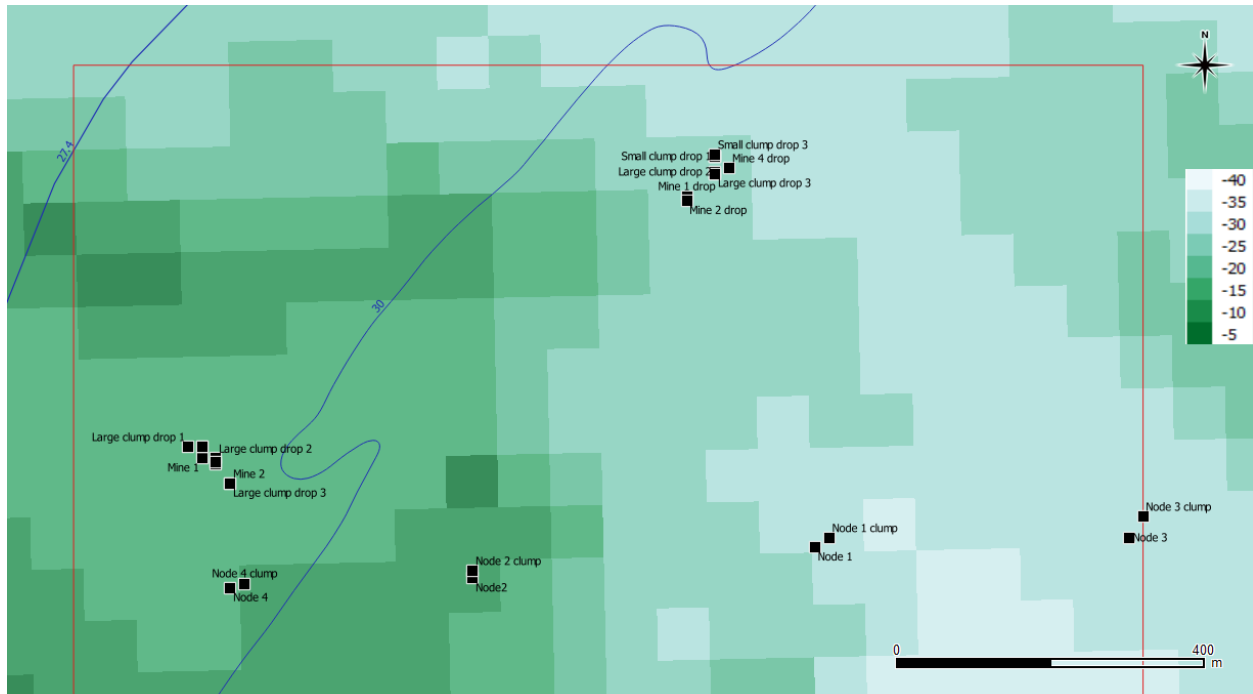
**Fig. 20 Detailed look at the sediment depth to bedrock, meters [Barnhardt et al. 2006] – zoomed in on the top section of the main box.. Note that the color-scale is recomputed at smaller increments. Range of values within the box: -8 to -37m below the seafloor.**

The overall depth of the sediment above the underlying bedrock is shown in Fig. 19. The range of depths for the main box is between approximately -36 and -6.5m below the seafloor. A close-up of the upper half of the main study box is shown in Fig. 20, where the color-scheme has been updated to increase resolution (smaller increment), as applicable to the minimum and maximum values (of bedrock depth below the seafloor), found in this region of interest.

Furthermore, if a 2D seismic propagation model is to be implemented, several linear profiles will be evaluated, originating at the target drop location (mine and mine-like objects) near the North-center part of the box (Deployment location 2) and terminating at each one of the node locations (nodes 3, 1, 2, and 4). Similarly, the profiles from Deployment Location 1 (near Western edge of the box) to all four nodes are also computed. These data are given in Fig. 21 and Fig. 22.
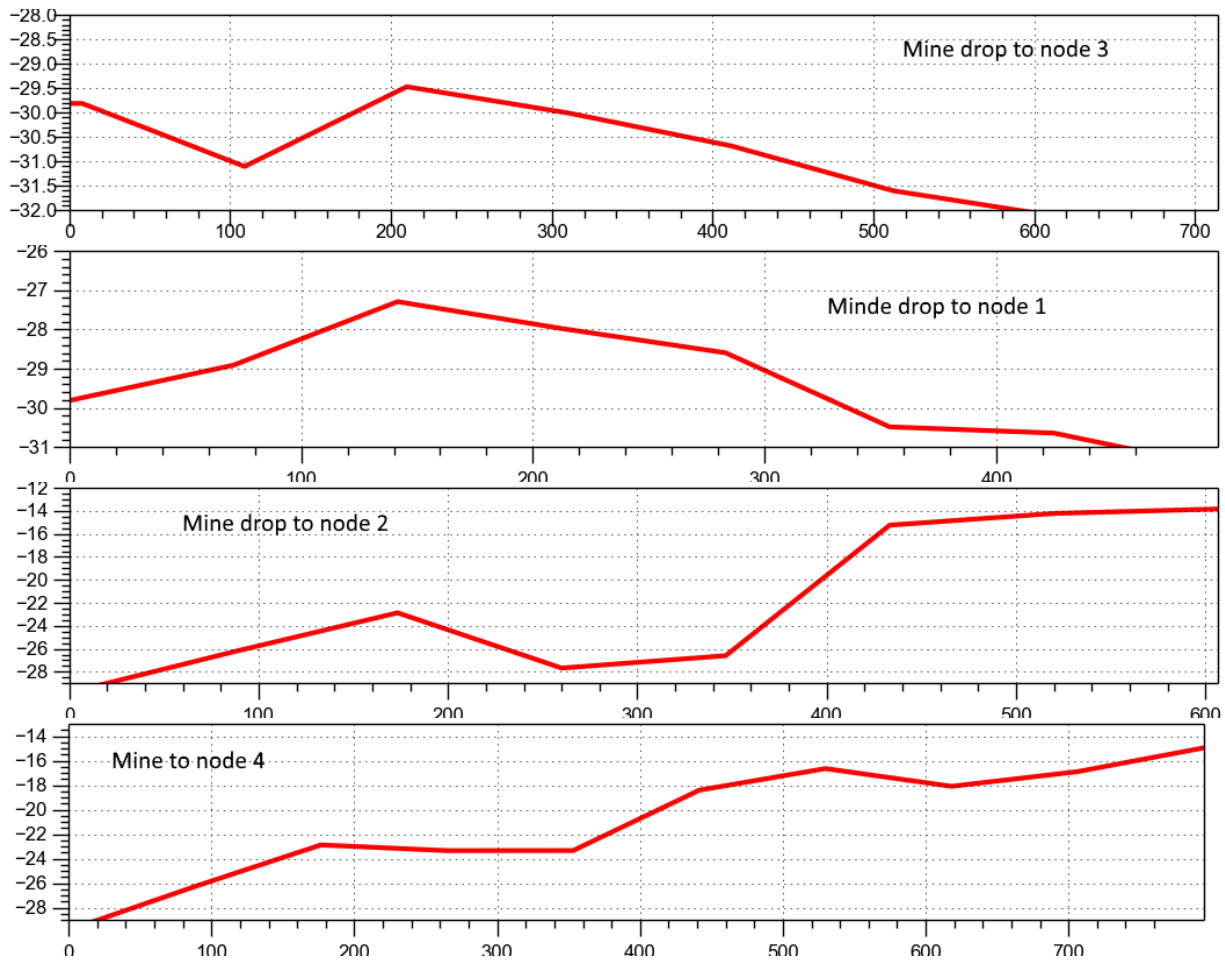
**Fig. 21 Sediment depth to bedrock, as interpolated from the USGS data: from mine drop location (2) to each of the four nodes**
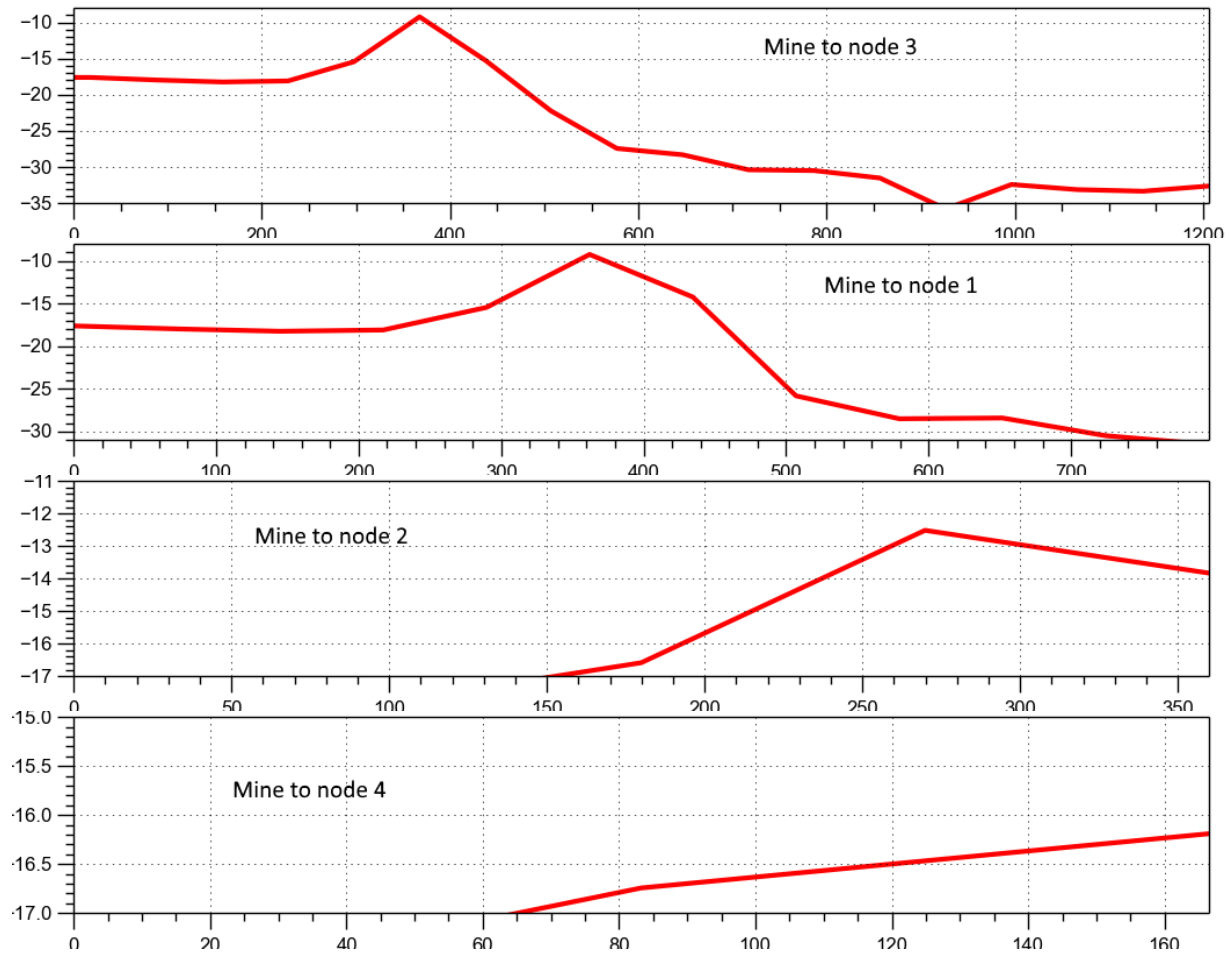
**Fig. 22 Sediment depth to bedrock, as interpolated from the USGS data: from mine drop location (1) to each of the four nodes**

### Layering from seismic survey

Several USGS/WHOI seismic surveys of the area are available and are summarized in Barnhardt et al. 2006.  The data was collected using a Knudsen 320b chirp system (3.5-12 kHz).  Several survey lines transect the area of interest.  Fig. 23 shows one such example line, in which, no apparent layering subsurface is observed (several surface reflection multiples).  Strong surface reflection, indicative of a coarse-grained packed surface layer is evident.
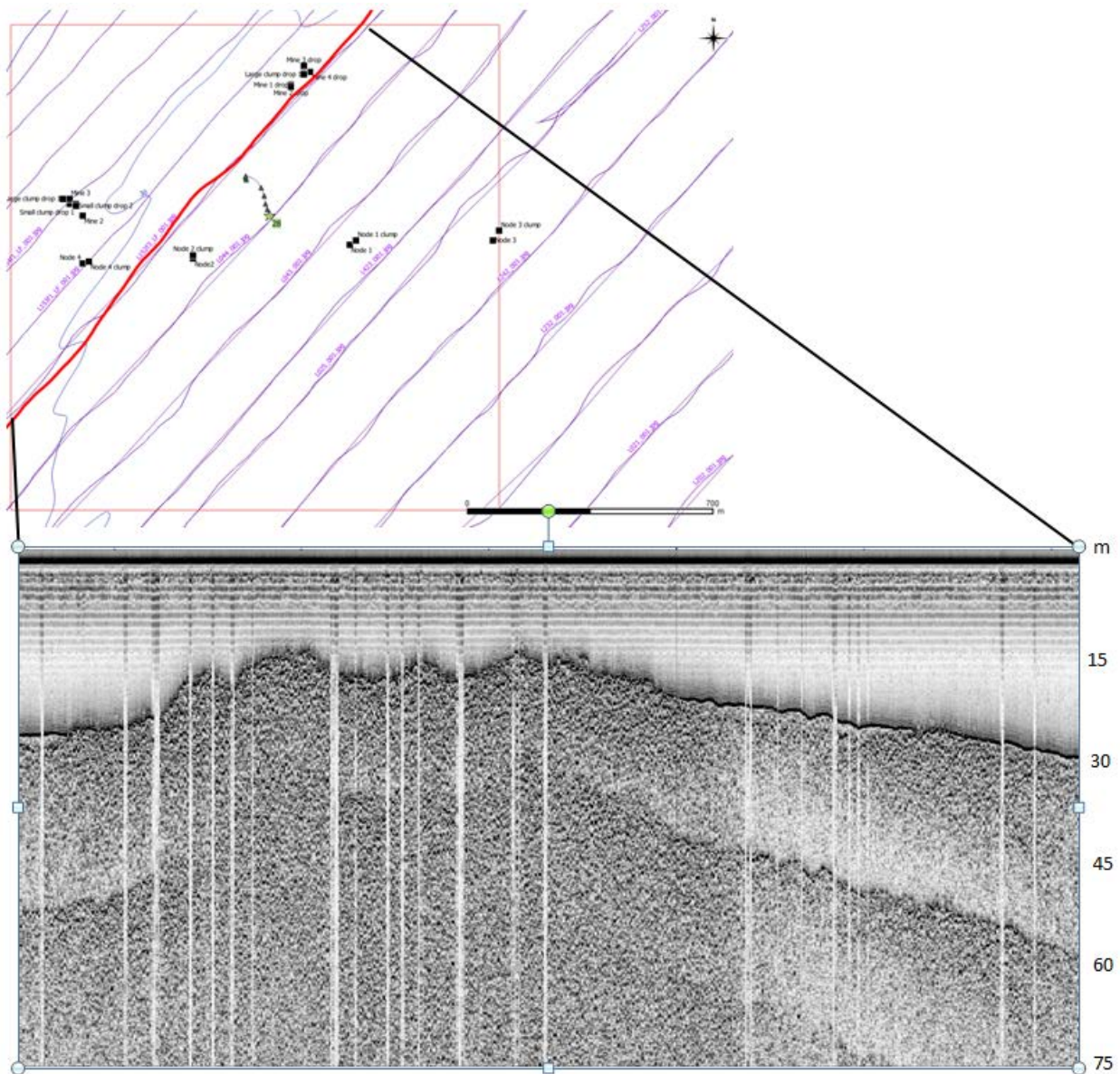


**Fig. 23  A seismic survey line through the main survey box, showing little observable stratigraphy (several multiples visible), indicating a generally hard sediment surface reflection [Barnhardt et al. 2006]**
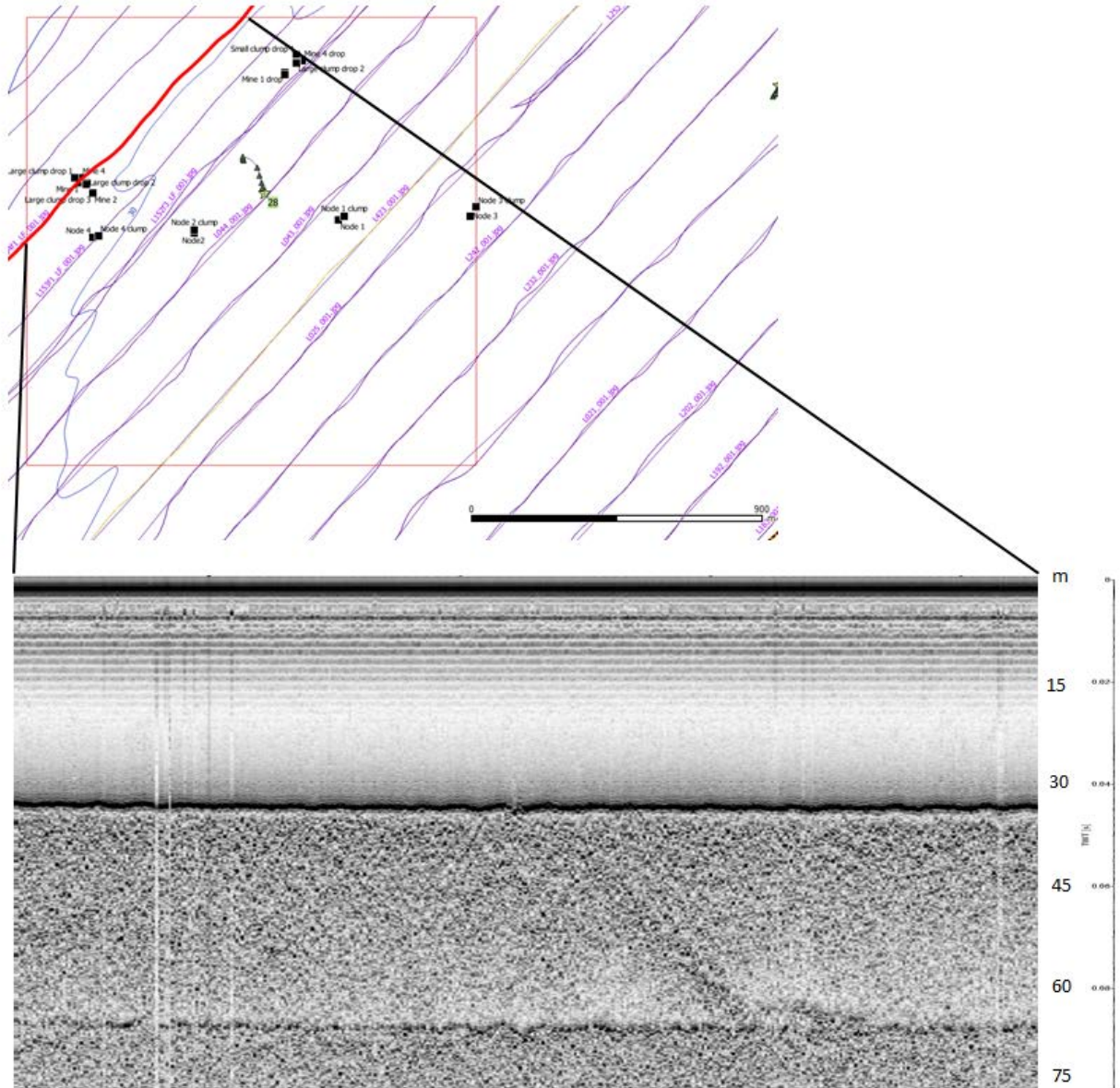
**Fig. 24 A seismic survey line through the main survey box (NW corner),showing a strong surface reflection and some apparent bedrock bottom with little other stratigraphy evident[Barnhardt et al. 2006]**

Fig. 24 shows another seismic profile from the same study, again, displaying a strong bottom surface reflection indicative of the hard surface sediment and low penetration energy into the seafloor. Some bedrock boundary is apparent and approximately coincides with the depth to bedrock map, generated in the source report. No other layering is apparent.

In conclusion, is appears safe to assume that there is little to no change in sediment type and properties down to the bedrock. We can, therefore, adopt a uniform set of material properties for the entire sedimentary layer in our propagation modeling.

# Summary

Exploration of the sediment surficial sediment composition and bearing strength as described by the STING free-fall penetrometers in Box 1 (Boston Harbor approach) indicates an overall highly heterogeneous material mixture of silt, sand, and gravel.  In general, it is difficult to make accurate estimates of the acoustic propagation properties such a heterogeneous area based on limited soil grab sampling (and lab grain-size analysis) and a STING data set.  Primary limiting factors may be considered the low spatial grab sample coverage, exacerbated by some difficulties in ship position keeping during sampling, as well as low material sampling volumes (small grab sampler).  The latter deficiency, results in potentially higher sample variability due to inability to sample sediment of this consistency (or strength) in depth, to at least the same penetration depth as those of the STING probes – approximately 20-50cm.

The analyzed data shows that the sediment is generally classified as Sand (primary fraction) with additions of gravel, especially increasing toward the North-most point of the area.  The sediment also seems to become slightly finer and with higher silt content toward the Eastern part of the box.  These effects are also traced in general in the STING data, indicating diminished penetration depth in coarse sediments and higher burials in sand-silt mixtures (East corner).

Estimated values of the sediment acoustic propagation properties may also be summarized as follows:

| Location in Area | Sediment Type | Compressional velocity (m/s) | Shear velocity (m/s) | Density (g/cm$^3$) | Attenuation factor, $k_p$[1] (dB/m/kHz) |
|---|---|---|---|---|---|
| North / North-Central | Coarser sand/fine gravel | 1800-1900[2] | 140 - 160 | 1.95 - 2.05 | 0.3 – 1.0[2] |
| Southwest/ South-Central | Sand | 1670-1750 | 90 – 140 | 1.90 - 2.00 | 0.2 – 1.0 |
| Southeast | Sand/silt | 1600 - 1730 | 80 - 100 | 1.70 - 1.85 | 0.3 – 0.8 |

It should be noted that the compressional and shear speed values were determined in tests at higher frequencies, e.g. 400kHz.  Sound speed appears approximately constant to about 10kHz (from higher values) and then decay by about 0.4—0.5 (sound speed ratio) for every log-cycle of frequency.

---

[1] see definition of $k_p$ in section: Shear wave speed
[2] estimated, based on an extrapolation of data, available in literature. No actual measurements are available for sediments of this range of the grain sizes.

Sound speed ratios (sediment vs. water) generally show frequency dependence as follows: 400 – 30kHz: approximately constant, followed by an approximately constant reduction in lower frequencies by 0.4 – 0.5 per log-cycle of frequency in kHz.

Attenuation shows a power-law dependency (for 5-500 kHz range) of approximately a log-cycle decay (dB/m) for a log-cycle reduction in frequency (in kHz).

Sediment depth to bedrock and sediment stratification were not explored during field testing, but inferred from available literature.  Overall, it appears that the area of Box 1 may be considered relatively uniform in depth but with highly variable sediment thickness over the bedrock.  Transects for acoustic/seismic propagation analysis were interpolated from the data available from USGS for all 2-D propagation paths form object drop locations and to all the sensor nodes on the seafloor.  These profiles could be used directly in any future modeling efforts as the boundary conditions.

**References**

ASTM Standard D422-63. (2007). "Standard Test Method for Particle-Size Analysis of Soils." ASTM International, West Conshohocken, PA.

ASTM Standard D2487. (2010). "Standard Practice for Classification of Soils for Engineering Purposes (Unified Soil Classification System)." ASTM International, West Conshohocken, PA.

Barnhardt, W. A., Andrews, B. D., and Butman, B. (2006). *High-resolution Geologic Mapping of the Inner Continental Shelf, Nahant to Gloucester, Massachusetts*. US Department of the Interior, US Geological Survey, Woods Hole Science Center.

Clay, C. S., and Medwin, H. (1977). *Acoustical oceanography: principles and applications*. Wiley.

Hamilton, E. L. (1976). "Shear-wave velocity versus depth in marine sediments: a review." *Geophysics*, 41(5), 985–996.

Hamilton, E. L. (1980). "Geoacoustic modeling of the sea floor." *The Journal of the Acoustical Society of America*, 68(5), 1313–1340.

Jackson, D. R., and Richardson, M. D. (2007). *High-Frequency Seafloor Acoustics*. Springer New York, New York, NY.

Jasco Research Ltd. (2002). *STING Mk.II - Underwater Sediment Bearing Strength Probe. User's Manual*. R-Hut, University of Victoria Campus Victoria, British Columbia.

Mulhearn, P. J. (2002). *Influences of penetrometer probe tip geometry on bearing strength estimates for mine burial prediction*. DTIC Document.

Pendleton, E. A., Barnhardt, W. A., Baldwin, W. ., Foster, D. S., Schwab, W. C., Andrews, B. ., and Ackerman, S. D. (2005). "USGS Open-File Report 2005-1293, High-Resolution Geologic Mapping of the Inner Continental Shelf: Nahant to Gloucester, Massachusetts, High-Resolution Geologic Mapping of the Inner Continental Shelf: Nahant to Gloucester, Massachusetts." <http://woodshole.er.usgs.gov/pubs/of2005-1293/html/maps.html> (Aug. 19, 2016).

Stoll, D., Sun, Y.-F., and Bitte, I. (2007). "Seafloor properties from penetrometer tests." *Oceanic Engineering, IEEE Journal of*, 32(1), 57–63.

Williams, K. L., Jackson, D. R., Thorsos, E. I., Tang, D., and Schock, S. G. (2002). "Comparison of sound speed and attenuation measured in a sandy sediment to predictions based on the Biot theory of porous media." *IEEE Journal of Oceanic Engineering*, 27(3), 413–428.

**Appendix A  STING data – bearing strength profiles with depth. Box 1.**

Note: negative bearing strength values that appear near zero sediment depth in some drops (or averages) are artefacts of STING software processing or minor inconsistencies in sensor calibrations and have no physical meaning.  This is possible in cases of very soft surficial material (as it is here), when the water-sediment interface is often not well defined and is difficult to determine from deceleration records (either via native automated STING processing or by manual selection).  Practically, these negative values should, of course, be all positive.  In all cases, these inconsistencies are minor and are well within the overall accuracy of the instrument in sediments of this type.

**Table 2 Results of STING tests (25mm foot). Positions for each sequence of drops are averaged and represented in this table with the average location and the position ID number corresponding to the first drop in series**

| PositionID | DateTime | PositionString | Description | AvePenDepth_m |
|---|---|---|---|---|
| 36 | 2016-01-06 15:12 | N42 26.277 W70 51.928 | STING34 | 0.32 |
| 37 | 2016-01-06 15:15 | N42 26.285 W70 51.899 | STING10 | 0.29 |
| 55 | 2016-01-07 12:45 | N42 26.443 W70 51.560 | STING10 | 0.19 |
| 58 | 2016-01-07 12:49 | N42 26.442 W70 51.559 | STING34 | 0.17 |
| 76 | 2016-01-07 19:56 | N42 26.240 W70 51.952 | STING10a | 0.29 |
| 80 | 2016-01-07 20:00 | N42 26.245 W70 51.942 | STING34a | 0.29 |
| 90 | 2016-01-07 20:50 | N42 26.219 W70 51.798 | STING10a | 0.17 |
| 94 | 2016-01-07 20:54 | N42 26.232 W70 51.795 | STING34a | 0.17 |
| 101 | 2016-01-07 21:27 | N42 26.263 W70 51.499 | STING10a | 0.10 |
| 105 | 2016-01-07 21:29 | N42 26.259 W70 51.505 | STING34a | 0.20 |
| 115 | 2016-01-07 22:01 | N42 26.233 W70 51.257 | STING10a | 0.39 |
| 119 | 2016-01-07 22:04 | N42 26.226 W70 51.264 | STING34a | 0.54 |
| 123 | 2016-01-08 13:29 | N42 26.345 W70 51.803 | STING10a | 0.30 |
| 127 | 2016-01-08 13:32 | N42 26.318 W70 51.759 | STING34a | 0.28 |
| 139 | 2016-01-08 15:01 | N42 26.337 W70 51.675 | STING10a | 0.17 |
| 143 | 2016-01-08 15:04 | N42 26.315 W70 51.766 | STING34a | 0.30 |
| 151 | 2016-01-08 15:26 | N42 26.317 W70 51.568 | STING10a | 0.11 |
| 159 | 2016-01-08 15:38 | N42 26.287 W70 51.599 | STING34a | 0.25 |
| 163 | 2016-01-08 15:50 | N42 26.319 W70 51.385 | STING10a | 0.27 |
| 171 | 2016-01-08 16:02 | N42 26.311 W70 51.459 | STING34a | 0.18 |
| 179 | 2016-01-08 16:15 | N42 26.260 W70 51.326 | STING10a | 0.28 |
| 183 | 2016-01-08 16:25 | N42 26.233 W70 51.467 | STING34a | 0.19 |
| 190 | 2016-01-08 16:37 | N42 26.209 W70 51.679 | STING10a | 0.24 |
| 194 | 2016-01-08 16:50 | N42 26.245 W70 51.683 | STING34a | 0.18 |
| 198 | 2016-01-08 17:01 | N42 26.262 W70 51.707 | STING10a | 0.21 |
| 205 | 2016-01-08 17:13 | N42 26.265 W70 51.717 | STING34a | 0.16 |
| 209 | 2016-01-08 17:25 | N42 26.422 W70 51.690 | STING10a | 0.15 |
| 216 | 2016-01-08 17:37 | N42 26.420 W70 51.700 | STING34a | 0.14 |
| 220 | 2016-01-08 17:52 | N42 26.420 W70 51.481 | STING10a | 0.21 |
| 227 | 2016-01-08 18:01 | N42 26.417 W70 51.503 | STING34a | 0.20 |

point: p36
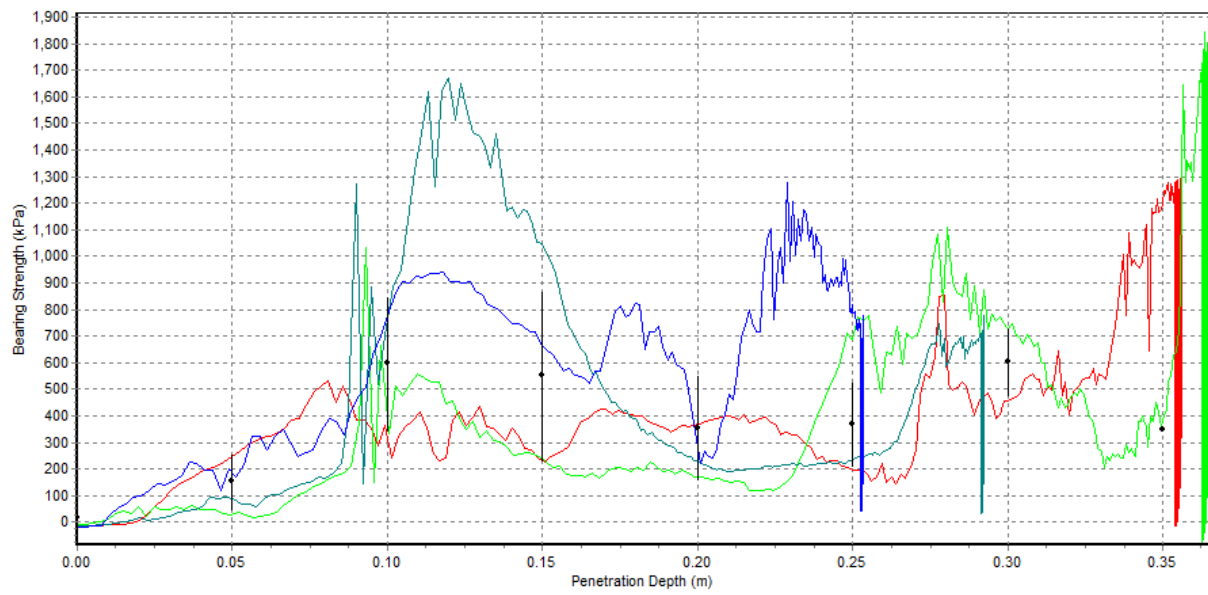


point: p37

point: 55



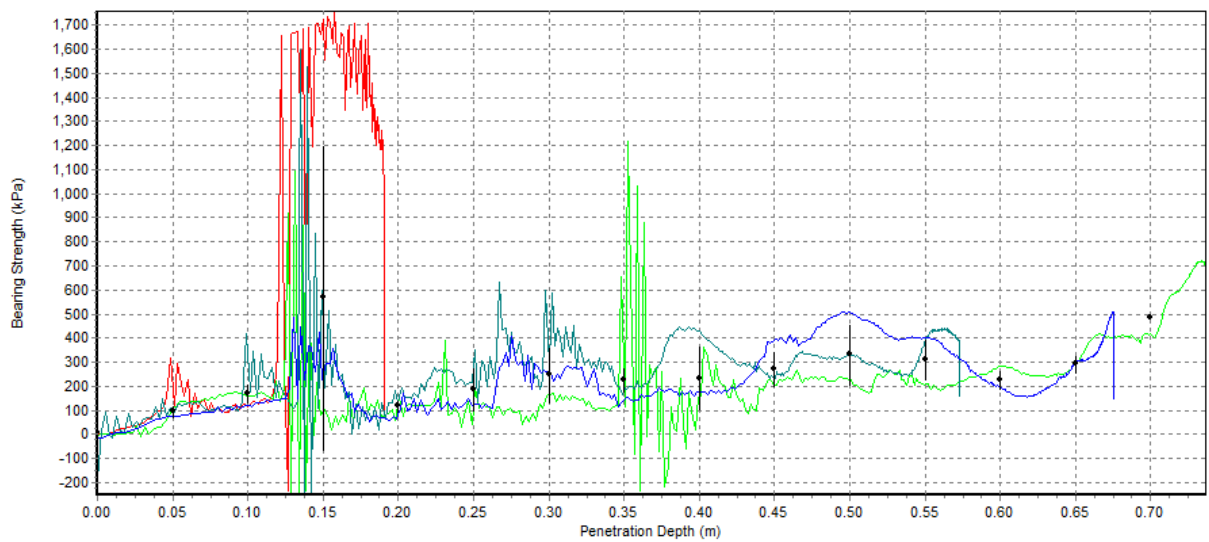point: 58



30
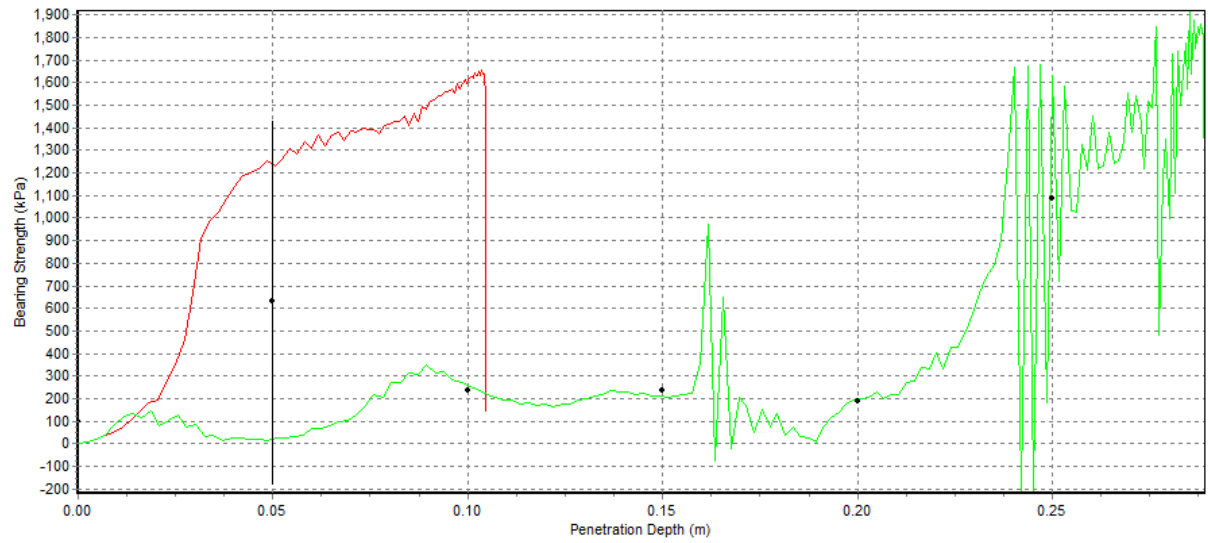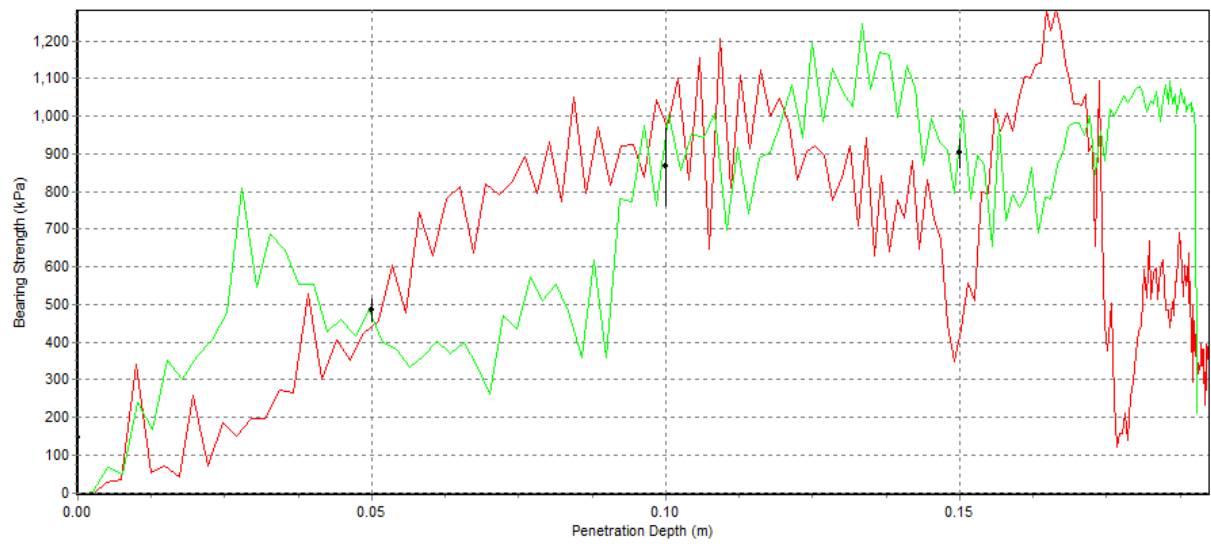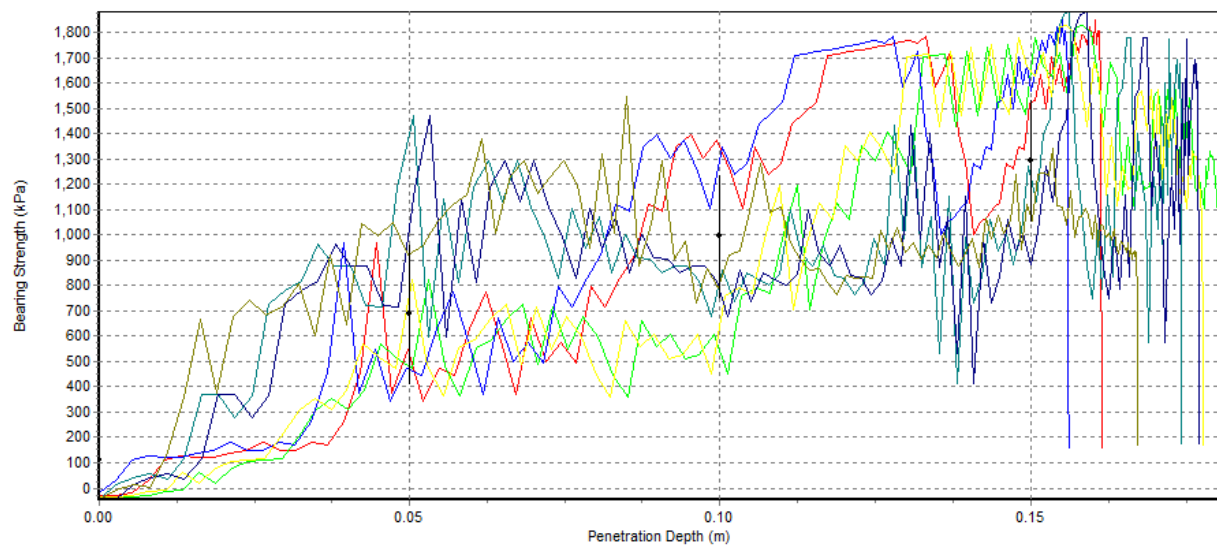
point: 76
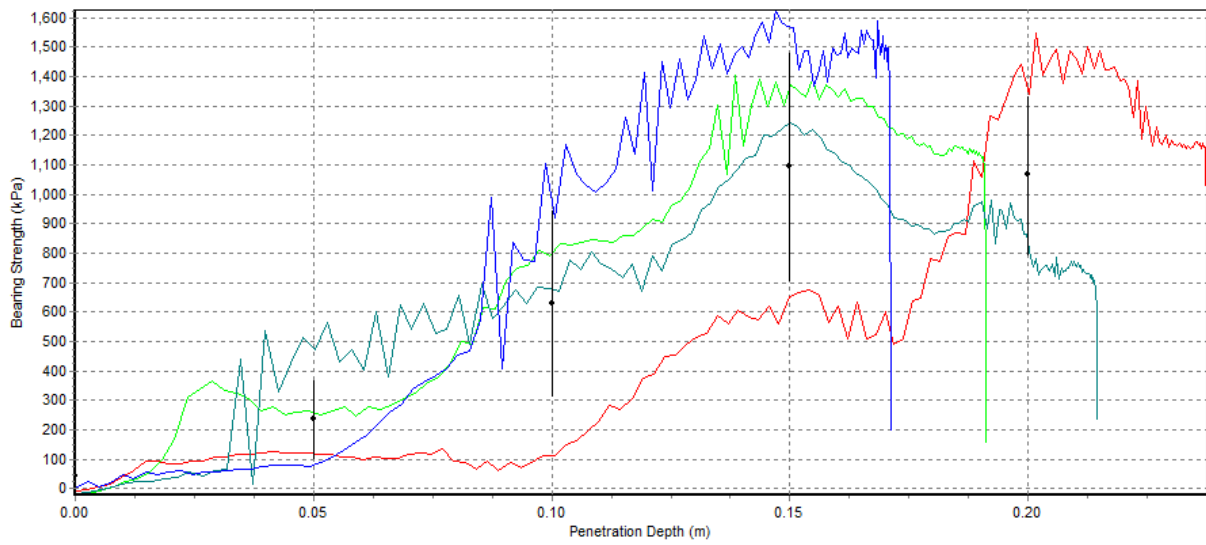


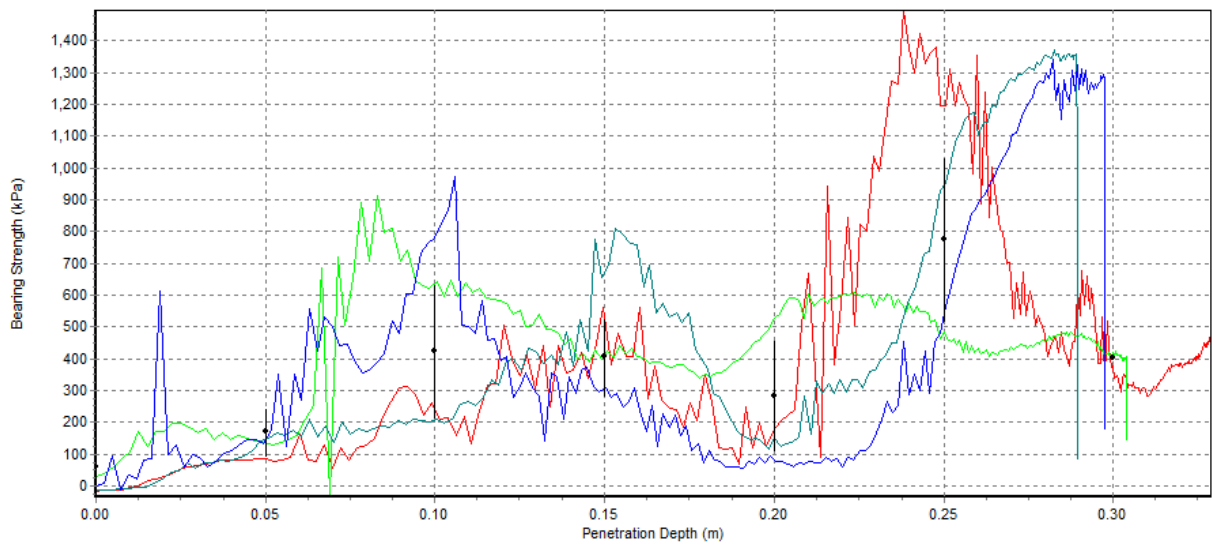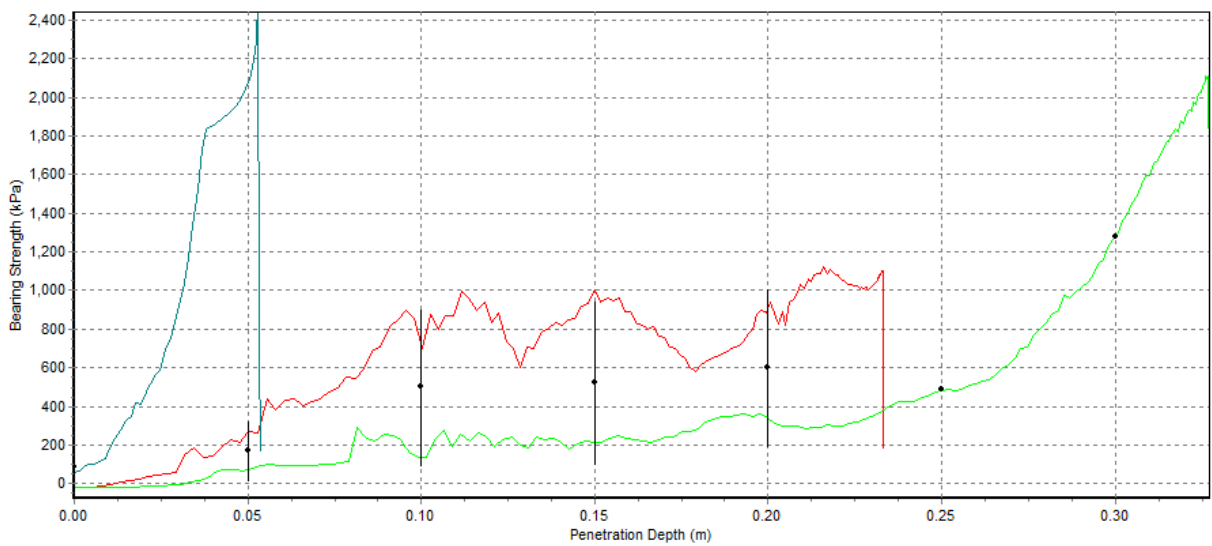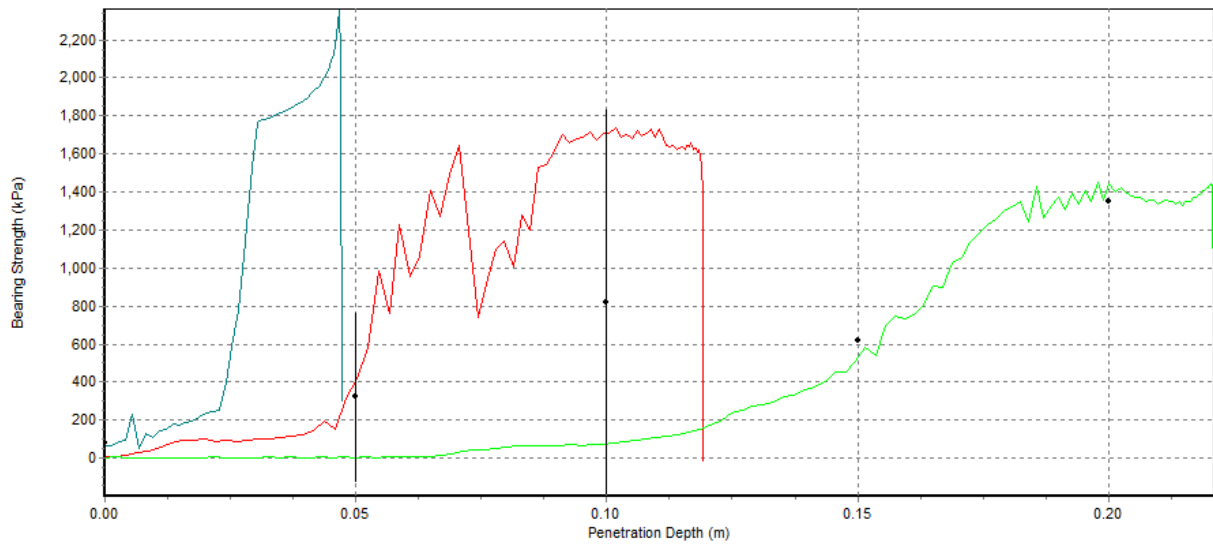point: 80
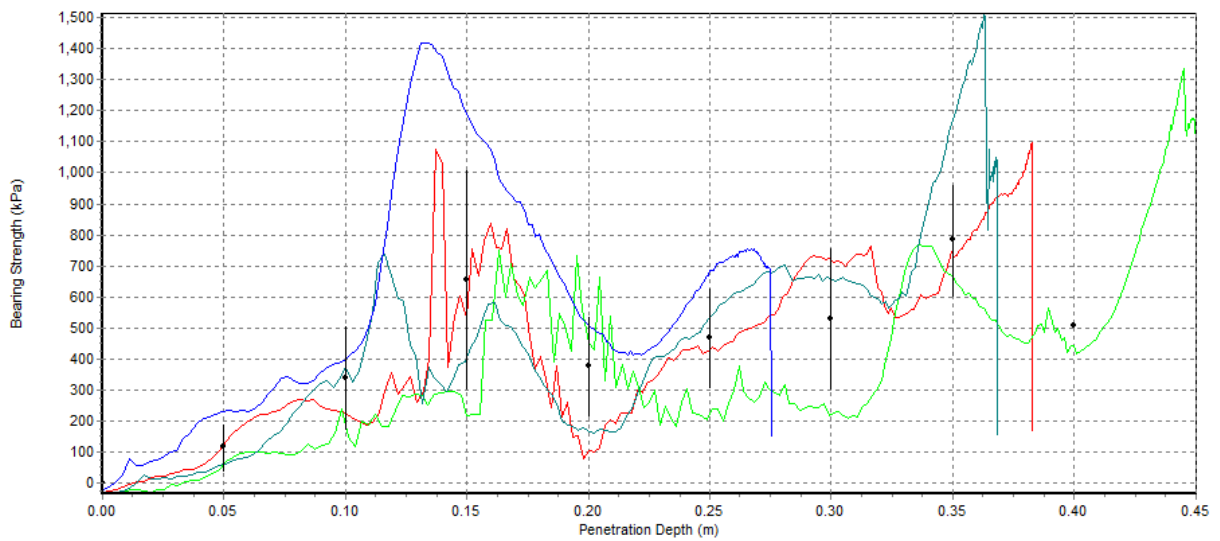
point: 90
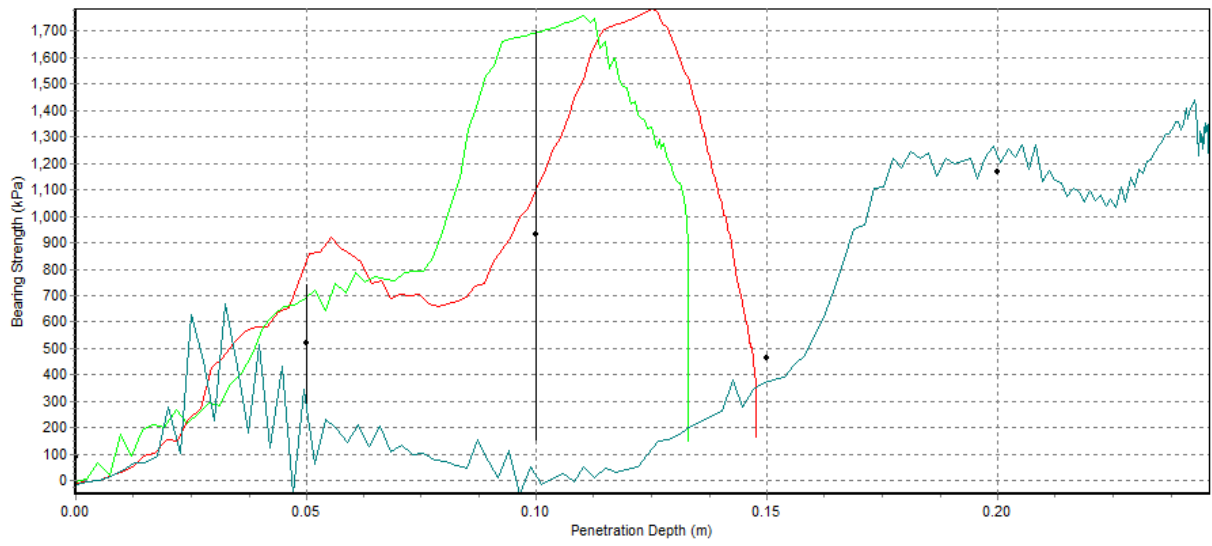


point: 94
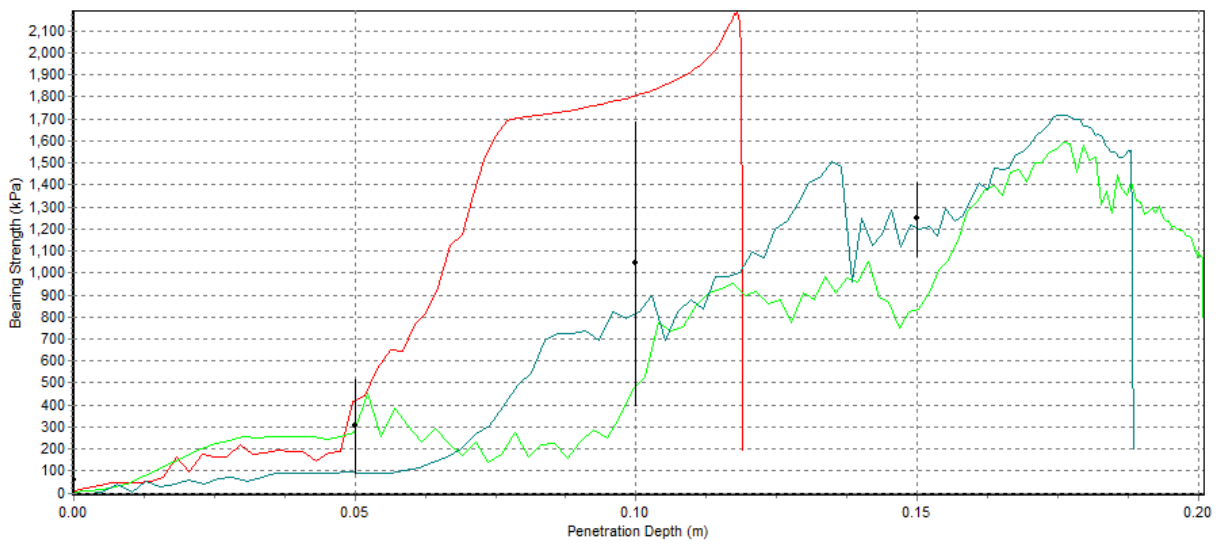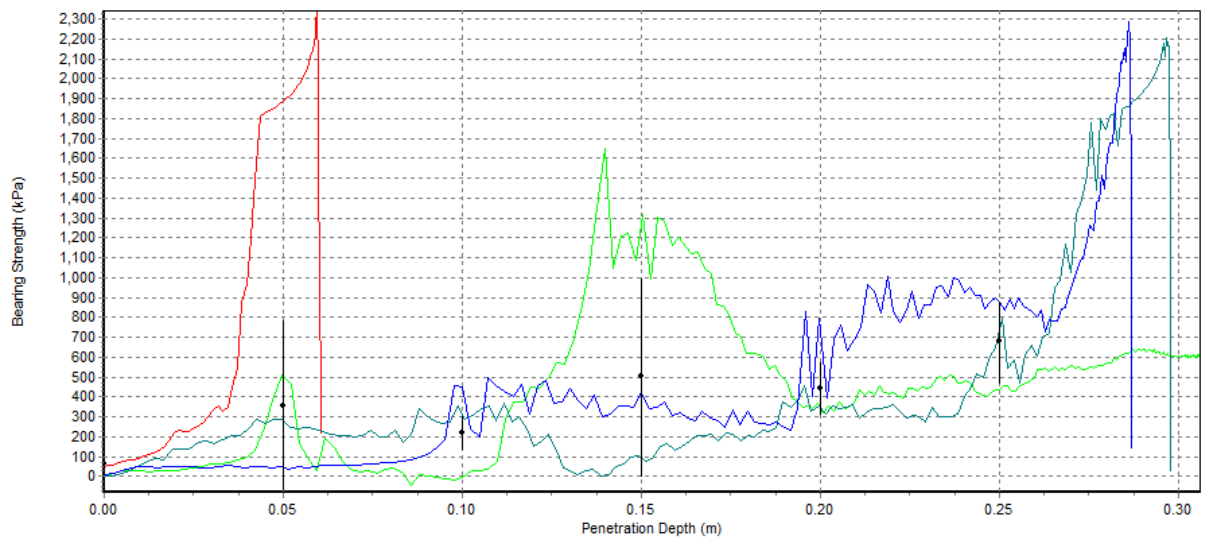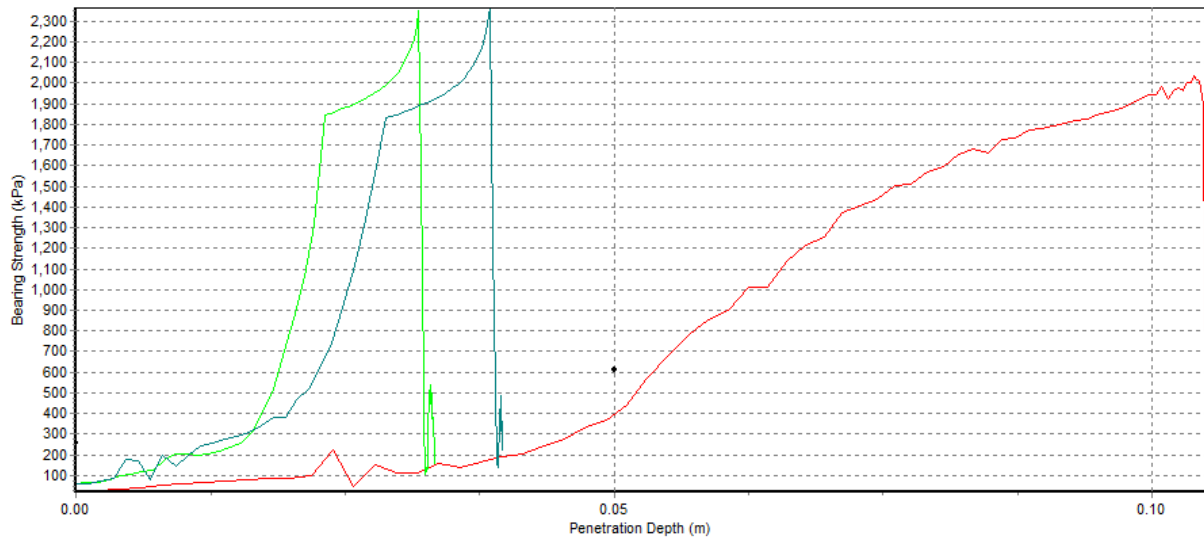
point: 101
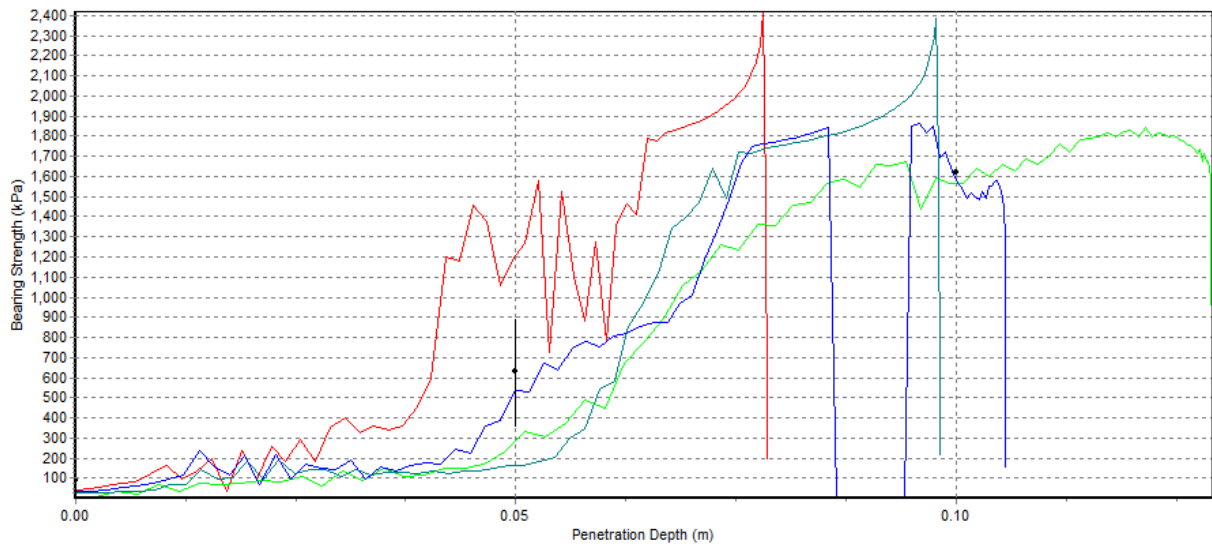


point: 108
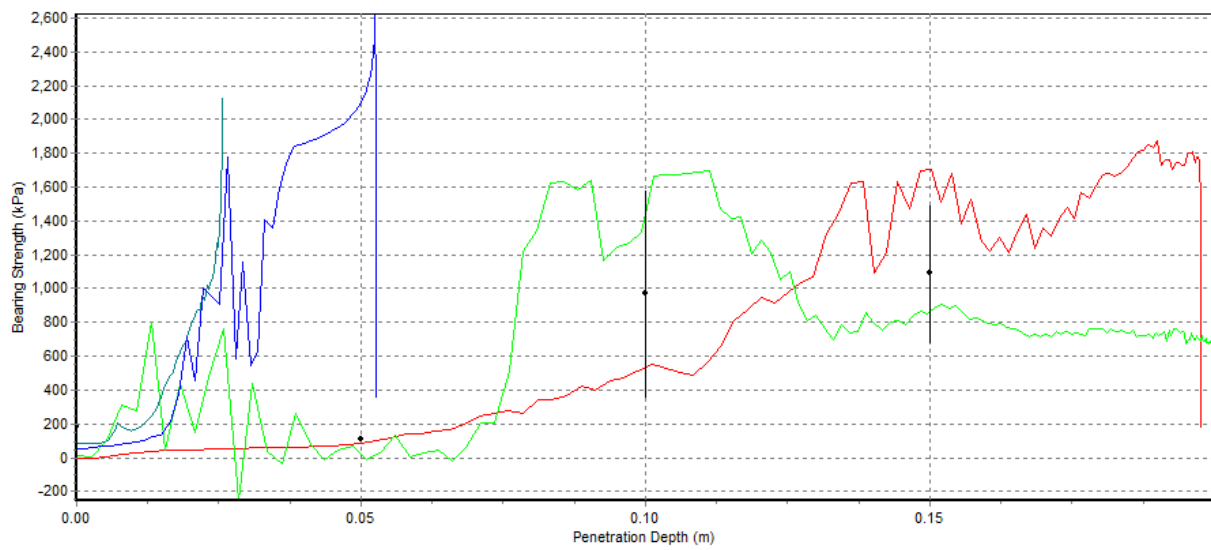
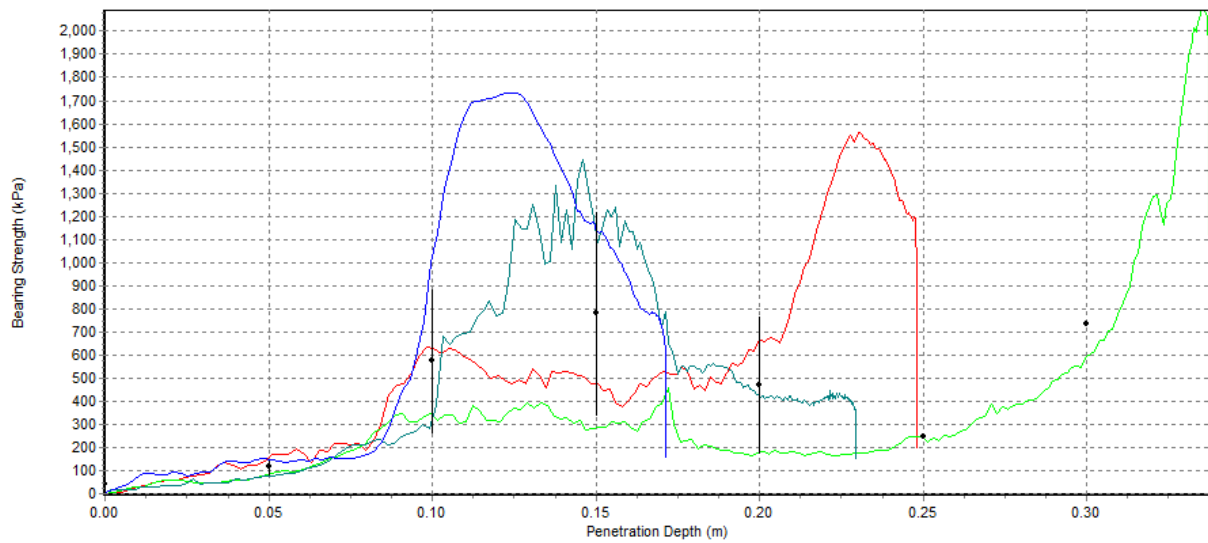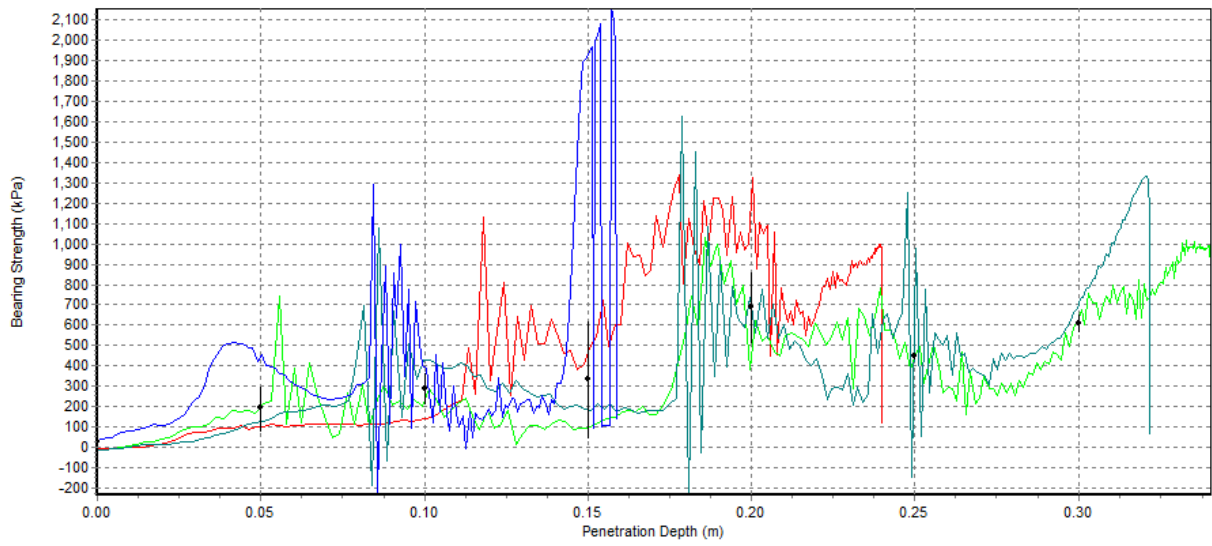point: 115



point: 119



34
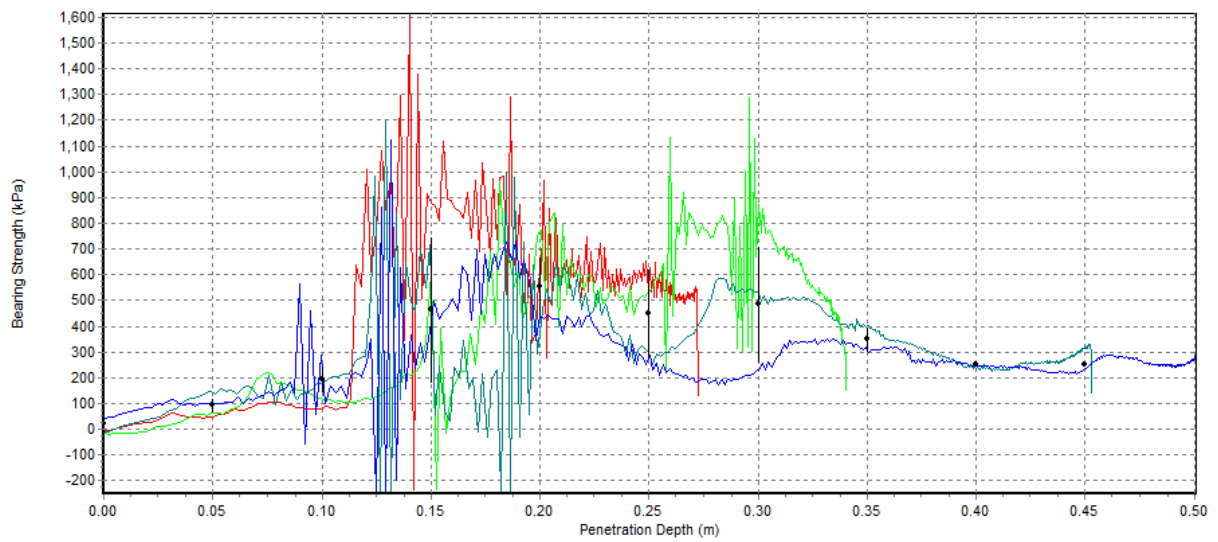
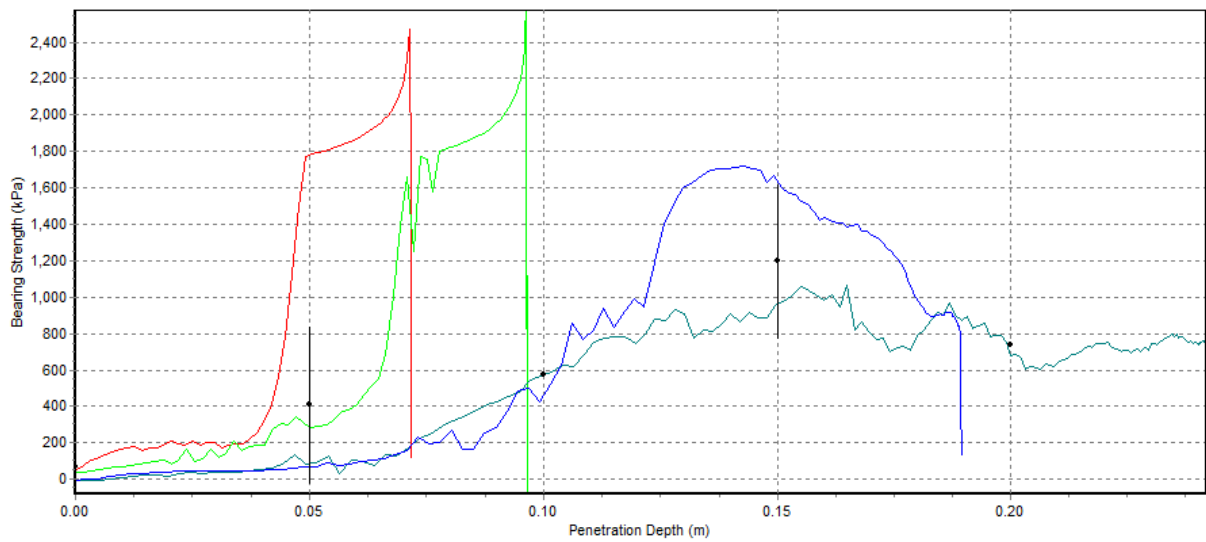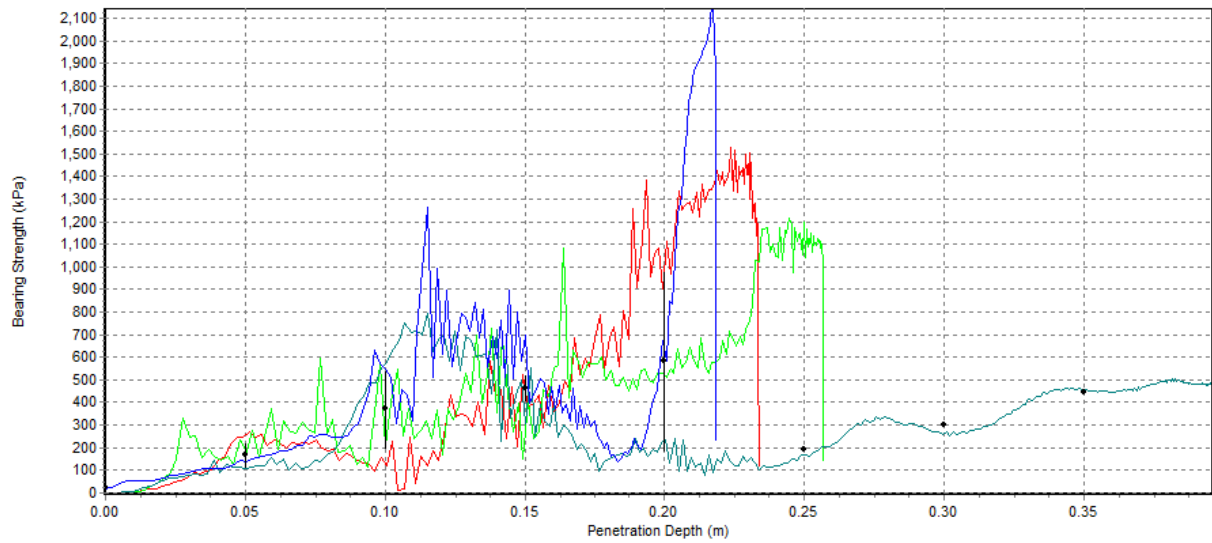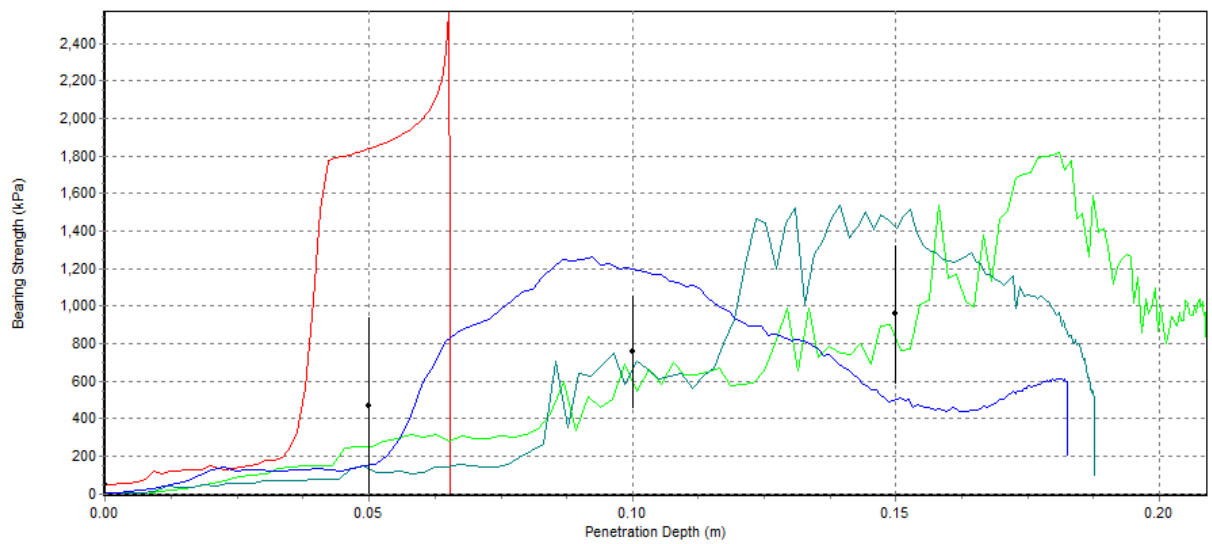point: 123



point: 127

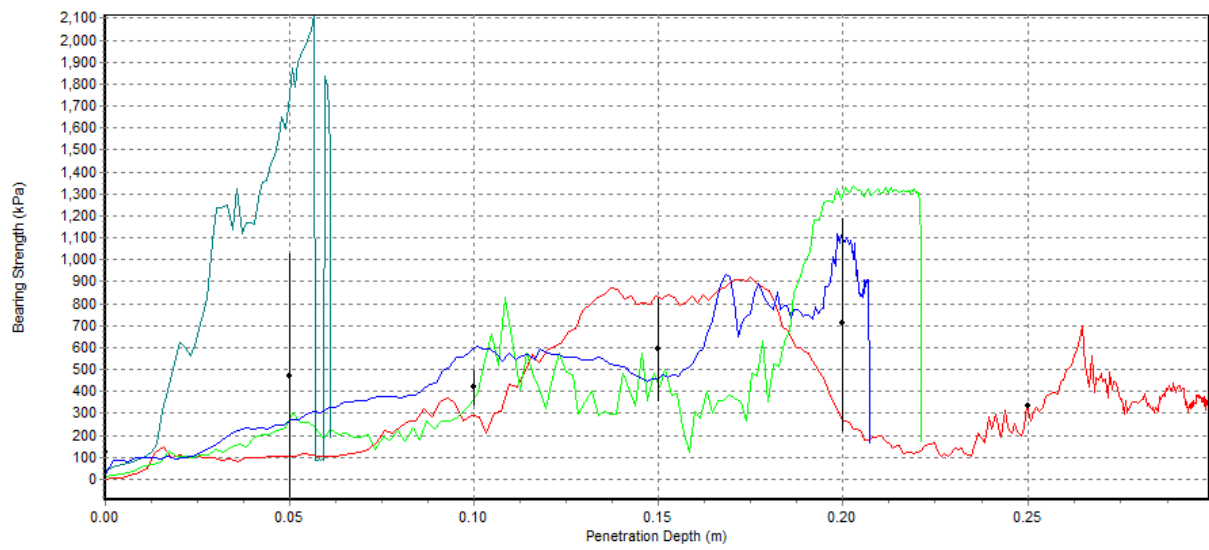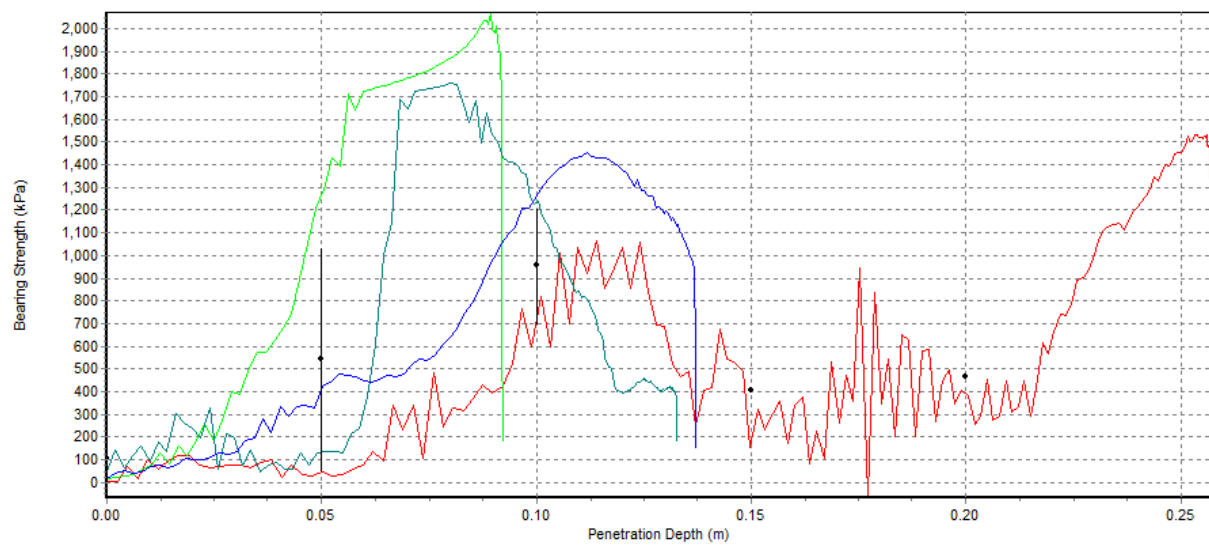point: 139



point: 143

point: 151
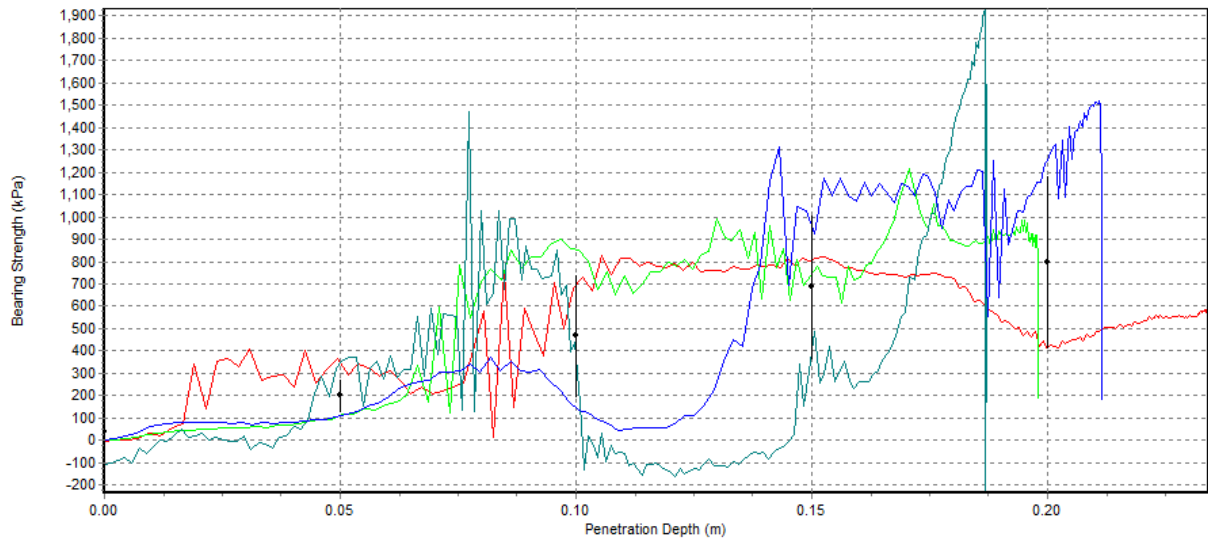


point: 159

point: 163



point: 171

point: 179



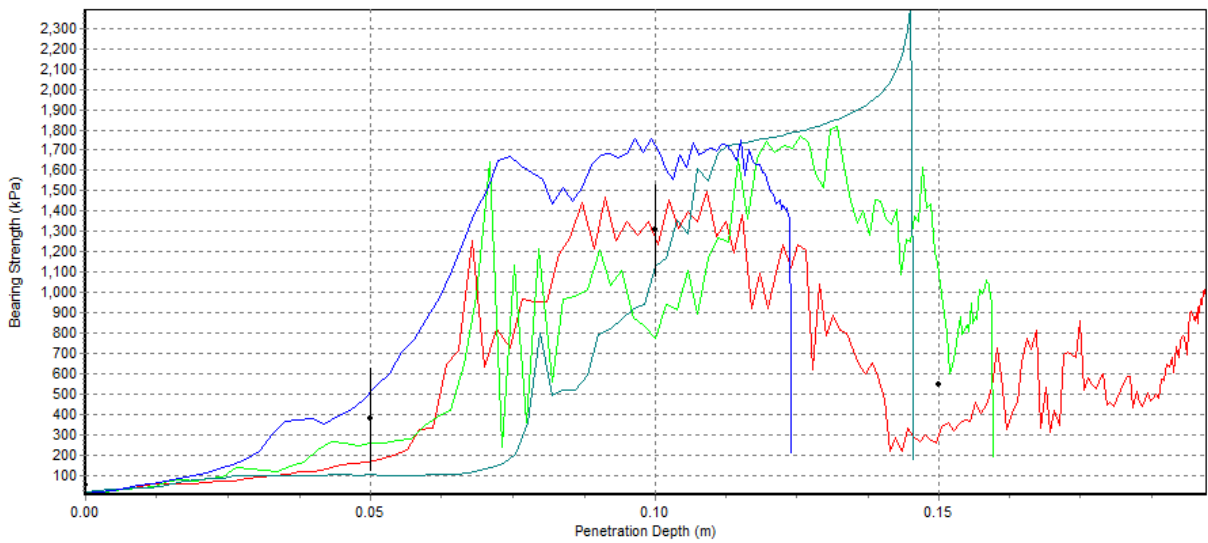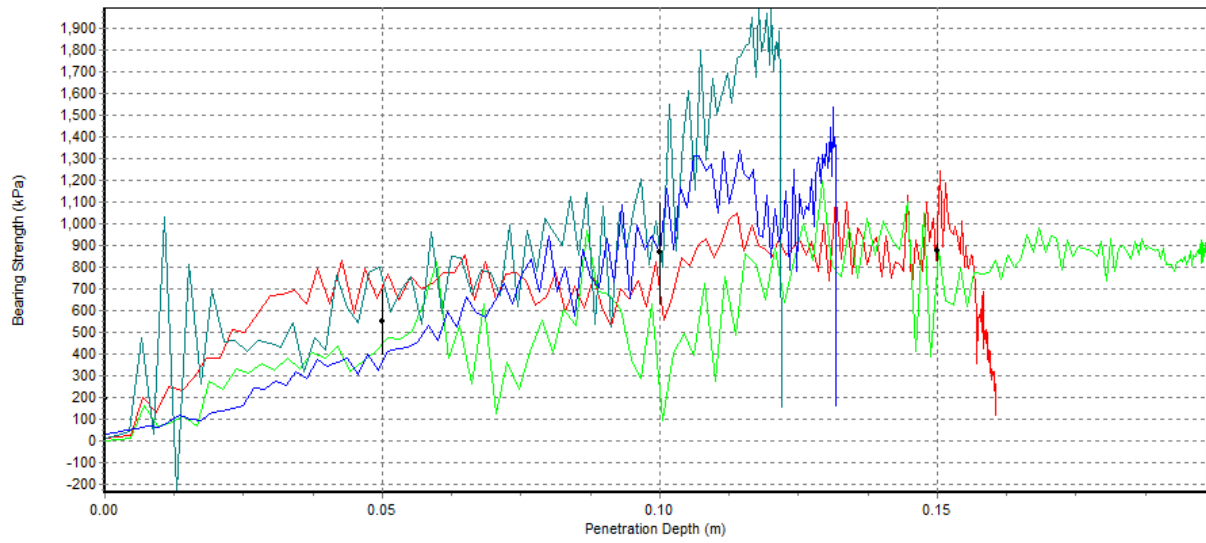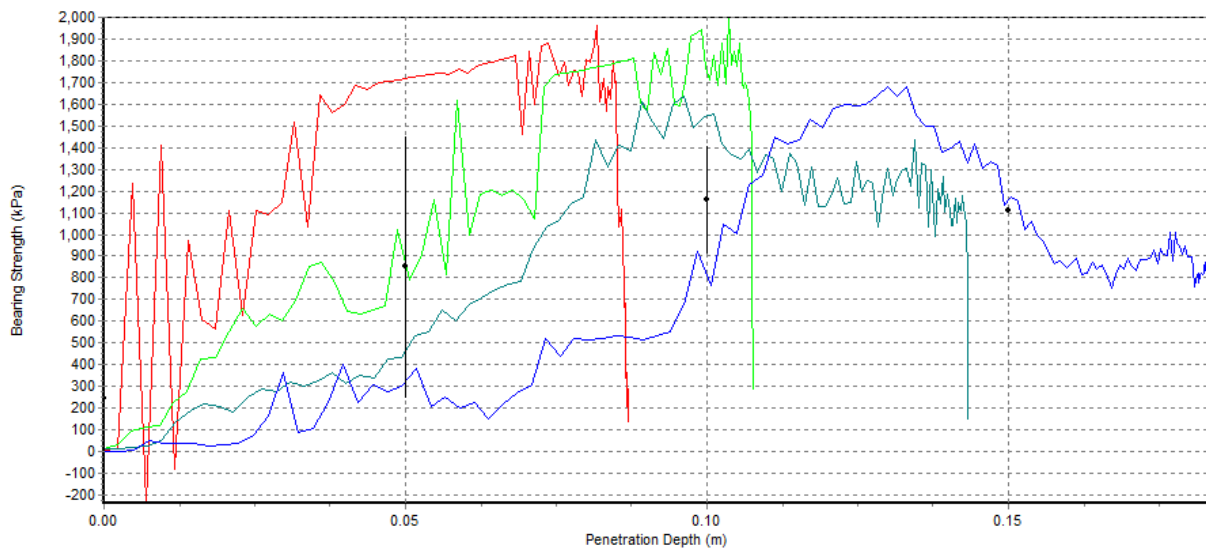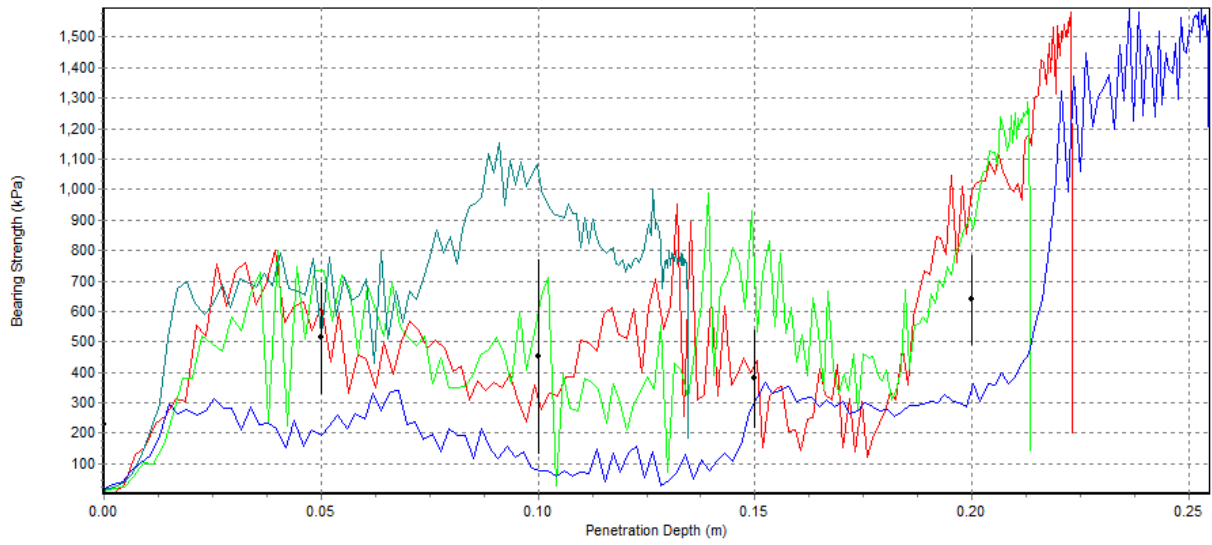point: 183

point: 190



point: 194

point: 198



point: 205

point: 209



point: 216

point: 220



point: 227